Development of a High Performance Concrete Deck for Louisiana's Movable Bridges: Numerical Study

Hadi Baghi Ph.D.[1], Fatmir Menkulasi Ph.D., P.E., A.M.ASCE[2], Jacob Parker P.E.[3], Joaquim A. O. Barros Ph.D.[4]

Abstract: Louisiana has approximately 160 movable bridges, mostly in the southern part of the state. This places Louisiana among the states with the highest inventory of movable bridges in the nation. The typical deck systems in these movable bridges are steel grids. Records show that steel grids have had maintenance issues. An alternative ultra-high/high performance concrete (UHPC/HPC) bridge deck system is proposed for Louisiana's movable bridges. This system consists of precast waffle slab deck panels, which are reinforced with glass fiber reinforced polymer (GFRP) bars as positive moment reinforcement, and a two-way carbon fiber reinforced polymer (CFRP) mesh as top reinforcement. Several validated nonlinear finite element analyses were performed to simulate the behavior of the precast panels from the onset of loading to failure. It is concluded that the precast concrete waffle slabs provide a viable alternative to steel grids by supplying load capacities that surpass service level and ultimate level load demands and deflection capacities that are within code specified limits.

[1]Post-doctoral Researcher, Department of Civil Engineering, Louisiana Tech University, Ruston, LA, 71272. Email: hadibaghi@gmail.com (corresponding author)

[2]Assistant Professor, Department of Civil and Environmental Engineering, Wayne State University, Detroit, MI, 48202. Email: fatmir.menkulasi@wayne.edu

[3]Structural Engineer, Stantec, Baton Rouge, LA. Email: Jacob.Parker@stantec.com

[4]Professor, ISISE, Department of Civil Engineering, University of Minho, Guimarães, Portugal. Email: barros@civil.uminho.pt

Introduction

Louisiana has approximately 160 movable bridges, mostly in the southern part of the state. This places Louisiana among the states with the highest inventory of movable bridges in the nation. These transportation arteries are important for the economic well-being of the state, as well as for the safety of the inhabitants in hurricane vulnerable regions during evacuations. Most of the movable bridges in Louisiana are either swing-span or lift-bridge type structures. Very few movable steel bridges are of the bascule type.

The typical deck systems in movable bridges are open steel grids, which typically consist of either diagonal or rectangular grids (Fig. 1). The diagonal grids were first used in the 1920s and represent the oldest lightweight deck system (Gase 2008). The traditional steel grid decks are supported by steel stringers at typically 1.22 m on center. On average these decks weigh less than 1.20 kN/m^2; while some others can weigh as little as 0.67 kN/m^2 (Mirmiran et al. 2009). This deck system is attractive because it is light weight, the panels are prefabricated and they are easy to install and replace. Also, deck crowning, scuppers, and drains are not required, since rain water drains through the openings in the deck (Mirmiran et al. 2009). Additionally, the light weight helps with imposing as little of a demand as possible on the mechanical system. However, records show that steel grids have exhibited durability issues. The proximity of these exposed steel systems to humid environments leads to rapid deterioration. As a result, decks become loose, causing extreme noise. Furthermore, inhabitants in areas close to movable bridges often complain about noise levels resulting from vehicles crossing over the steel grids. These problems are aggravated by trapping foreign debris throughout the deck grids. The lack of traction in steel grid decks is another concern with respect to safety.

The Louisiana Department of Transportation and Development (LADOTD) has an interest in using concrete decks to replace deteriorated steel grids on existing movable bridges as well as in new construction. However, the mechanical systems of moveable bridges are highly sensitive. As a result, any decking used to replace or rehabilitate the existing steel grid decking should match the weight of the existing steel grid such that the mechanical system operates as designed. The weight to strength ratio of conventional concrete decks will have a negative impact on the load demand imposed on the mechanical system. Accordingly, a light ultra-high/high performance concrete (UHPC/HPC) deck is proposed as an alternative to steel grid decking. The current definition of UHPC under review in the technical committee of the American Concrete Institute (ACI 239) (2015) is: “Concrete that has a minimum specified compressive strength of 150 MPa with specified durability, tensile ductility and toughness requirements; fibers are generally included to achieve specified requirements”. High-performance concrete is defined as concrete meeting special combinations of performance and uniformity requirements that cannot always be achieved routinely using conventional constituents and normal mixing, placing, and curing practices (ACI CT 2013). The UHPC/HPC deck system is intended to provide a continuous driving surface that mimics monolithic construction, provides integral connections with the supporting stringers as well as between adjacent deck panels, and provides traction, which should improve traffic safety.

Florida Department of Transportation (FDOT) in collaboration with URS Corporation identified several potential alternative lightweight solid deck systems to replace steel open grid decks on typical Florida bascule bridges (Mirmiran et al. 2009; 2012; Phillips 2014; and Mirmiran and Ghasemi 2016). These deck systems include a sandwich plate system, a fiber reinforced polymer (FRP) composite deck, an aluminum orthotropic deck, a prismatic concrete deck with

FRP tubes, a non-prismatic concrete deck with FRP tubes, a FRP deck, and a waffle slab UHPC deck. The sandwich plate system and the FRP composite systems are vulnerable to delamination, debonding and cracking of wearing surface. The aluminum orthotropic deck is a patented product, and requires expansion joints, periodic replacement of the wearing surface, galvanic corrosion mitigation, as well as the potential use of blind-type fasteners (Mirmiran et al. 2009). The UHPC deck with FRP tubes was not investigated with respect to the performance of panel to stringer connections, panel to panel connections, and fatigue performance of the system. The deflection of the FRP deck system under service load significantly exceeded the deflection limit suggested by the American Association of State and Transportation Officials (AASHTO) Load and Resistance Factor Design (LFRD) Specifications (2014) (Article 9.5.2). The stiffness of the FRP deck was enhanced by adding an UHPC layer on the top. The dominant mode of failure in the FRP deck with an UHPC overlay was either at the interface of FRP and UHPC, or through buckling of the FRP web.

The UHPC waffle slab system was investigated further by Mirmiran et al. (2012) and Mirmiran and Ghasemi (2016). Both $MMFX_2$ bars and carbon fiber reinforced polymer (CFRP) bars were investigated as reinforcement alternatives for the waffle slab configuration. The overall thickness of the waffle slab configuration varied from 102 mm to 127 mm, and the spacing between the stringers was 1.22 m. The weight limitation was 1.01 kN/m^2. The waffle slab configuration proved to be a viable alternative to steel grid decks for Florida's movable bridges by meeting AASHTO's (2014) load demands.

As it will be described in the next section there are some differences between the characteristics of the steel grid decks in Florida compared to those in Louisiana. The predominant depth of the existing steel grids in Louisiana is 132 mm compared to the 102-127 mm range investigated in

Florida. The maximum weight limitation for Louisiana's movable bridge decks is 0.96 kN/m^2 compared to the 1.01 kN/m^2 weight limit for Florida's bascule bridge decks. The majority of movable bridges in Louisiana featured steel grid spans, defined as the distance between the centerlines of stringers, less than or equal to 1.27 m compared to 1.22 m in Florida. At first glance these differences may appear small or negligible taking into the consideration the accuracy typically employed in structural engineering work. However, given the strict limitation on the maximum weight imposed on the mechanical system, such small differences required the development of a unique deck configuration for Louisiana's movable bridges. The UHPC deck configuration developed in Florida, while viable for Florida's bascule bridges could not be directly applied to Louisiana's movable bridges for the following reasons: 1) the maximum weight limit is greater than that determined for Louisiana's bridges, 2) the depth of the deck was shallower than the predominant depth recorded for Louisiana's bridges, thereby increasing the overall depth would further exceed the maximum weight limit, 3) the span between the centerlines of stringers is 51 mm shorter than that determined for Louisiana's bridges.

Aaleti et al. (2011; 2013) developed an UHPC waffle slab for non-movable bridges. There was no limitation on the maximum weight of the deck. The overall depth of the slab was 203 mm. The thickness of the flange was 64 mm and the thickness of the transverse ribs varied from 76 mm at the bottom to 102 mm at the top. The range of spans considered varied from 1.22 m to 3.05 m. The weight of this deck system far exceeds the maximum weight limitation for Louisiana's movable bridges (0.96 kN/m^2) because the deck configuration was developed for non-movable bridges. However, the female-to-female type panel to panel connections provided a good starting point and are similar to the detail proposed for Louisiana movable bridges.

The goal of this research is to develop an UHPC/HPC deck system for Louisiana's movable bridges. A modified version of the waffle slab UHPC deck investigated in Florida is proposed for investigation in this study because: 1) it can meet the limitations on weight and overall depth for Louisiana's movable bridges, 2) it can meet load and deflections demands specified in AASHTO (2014), 3) it uses high strength corrosion resistant reinforcement, 4) it uses panel to panel and panel to stringer connections that are intended to emulate monolithic action, and 5) it includes either a chip seal surface coating or a controlled broom finish to provide skid resistance and increase traction.

Compilation of Louisiana's current moveable bridge deck system details

A list of movable bridges that utilize steel grid decking was obtained from LADOTD. The bridge plans including as-built drawings and shop drawings were searched to collect all relevant information such as: panel thickness, panel weight, panel length, cantilever length, span length, and stringer size. Cantilever length was defined as the distance from the centerline of the exterior stringer to the edge of the steel grid. Span length was defined as the distance between the centerlines of stringers. The bridge plans for a total of 17 bridges were investigated during the period of time allocated to complete this task. The minimum and maximum deck thickness were 129 mm and 150 mm, respectively. The predominant deck thickness was 132 mm. There was a minimum deck weight requirement only for two bridges (0.77 kN/m^2 and 0.84 kN/m^2). The maximum deck weight limitation based on stringer reactions was typically 0.96 kN/m^2 with the exception of one bridge for which this limitation was 0.86 kN/m^2. The most common stringer type was W410×54. The spacing of stringers varied from 1.12 m to 1.42 m, however the majority of bridges featured stringer spacing less than or equal to 1.27 m.

Based on the collected information the following recommendations were made with the respect to the development of UHPC deck panels (Table 1). The panel thickness is recommended to be

132 mm to be consistent with the predominant existing grid deck thicknesses. The maximum panel weight should be limited to 0.96 kN/m^2 so that specified maximum stringer reactions are not exceeded. The span length should be 1.27 m to cover the majority of the investigated bridges. The panel length should be such that it covers at least three spans to take advantage of continuity and reduce the number of joints exposed to traffic. Alternatively, continuity for superimposed loads in the transverse direction can be achieved by placing a site cast UHPC/HPC diaphragm between the ends of the individual precast waffle slab deck panels. This detail is illustrated in the next section. The stringer size that should be considered during the development of the UHPC deck is W410×54 because this was the most common size.

Proposed Precast Deck System

The proposed system is illustrated in Fig. 2, 3 and 4. Two deck configurations are investigated with respect to the number of longitudinal ribs. These two deck configurations (denoted as Deck System 1 and Deck System 2 in Fig.2a) were determined based on preliminary work performed by Menkulasi et al. (2016). In the first configuration there is only one partial depth longitudinal rib at mid-span of the panel, which helps distribute loads to the adjacent ribs. The dimensions of this partial depth rib are 22 mm wide and 70 mm deep from the bottom of the top flange. In the second configuration there are a total of six partial depth longitudinal ribs. The width of these ribs is 22 mm whereas the depth is 19 mm. Both panel configurations will receive a chip seal surface coating or a controlled broom finish to provide traction. The weight of the chip seal surface coating is negligible.

Continuity for live loads in the transverse direction is achieved by placing a cast-in-place (CIP) UHPC/HPC diaphragm between the ends of the precast deck panels when they are fabricated as single span panels (Fig. 2a and Details C1a and C2a in Fig. 3 and Fig. 4). There is a distance of 24 mm between the end of the panels and the centerline of the stringers to allow for the placement of the cast-in-place UHPC/HPC diaphragm. The top flange at the ends each panel is coped 76 mm in length and 11 mm in depth to allow the C-grid to project past the ends of the panels, be immediately above the coped flange and lap with the C-grid from the adjacent panels. The C-grid projects 76 mm past the ends of the panel to create a 152 mm lap with the grid coming for the adjacent panel (Details C1a and C2a in Fig. 3 and Fig.4). All the interfaces between precast and cast-in-place UHPC/HPC in the proposed connections should be sandblasted and kept moist at surface saturated dry conditions to enhance bond.

When deck panels are fabricated such that they cover two or more spans the details will be similar with the exception that the flange and transverse ribs will be continuous over the supports and the cast-in-place concrete diaphragm will be placed through access holes from the top of the precast deck (Fig. 2b and Details C1b and C2b in Fig. 3 and Fig. 4).

Continuity in the direction of traffic is provided by using female-to-female type panel to panel connections and a cast-in-place UHPC/HPC fill (Details B1 and B2 in Fig. 3 and Fig.4). The steel stringers are spaced at 1.27 m on center. The width of a single precast panel is 1.22 m. The overall depth of the deck panels is 132 mm. The thickness of the flange is 22 mm. The width of the transverse ribs, which will act as T-beams to support the superimposed loads varies; it is 51 mm at the bottom of the stem and it tapers down to 22 mm (Details A1 and A2 in Fig. 3 and Fig. 4). The width of end ribs at the bottom is equal to 38 mm for deck configuration 1 and 32 mm for deck configuration 2.

The spacing of the transverse ribs is 406 mm center to center for the interior ribs and 406 mm from the center of the interior rib to the outside face of the exterior rib. The weight of a single panel considering the cast in place UHPC/HPC diaphragm is 0.964 kN/m^2 for deck system 1 and

0.955 kN/m^2 for deck system 2. The weight of deck system 1 is slightly over the target weight of 0.96 kN/m^2 and was calculated using a measured unit weight of 2500 kg/m^3 for *Ductal*. *Ductal* is a commercial UHPC/HPC formulation provided by Lafarge North America and was supplied to the research team by Lafarge as part of this study. The panel weight was calculated by ignoring the presence of the reinforcement bars and mesh because the unit weight of reinforcement was less than that of concrete.

Glass fiber reinforced polymer (GFRP) bars (GFRP V-ROD HM - 60GPa Grade III) are proposed as positive moment reinforcement in the transverse and longitudinal ribs. GFRP bars are corrosion resistant and are produced by Pultrall Inc. Each interior transverse rib is reinforced with a No. 16 GFRP bar at the bottom and each exterior rib is reinforced with a No. 13 GFRP bar. The partial depth longitudinal ribs in both configurations are reinforced with a No. 10 GFRP bar to help distribute wheel loads in the longitudinal direction. The clear bottom cover to positive moment reinforcement is 11 mm in the interior ribs and 10 mm in the exterior ribs. The clear cover in all other cases is equal to 6 mm or greater.

Flange reinforcement consists of a two-way non-corrosive carbon fiber grid (C-grid) developed by Chomarat North America. C-grid is an epoxy-coated composite grid made with cross-laid and superimposed carbon fiber. The diameter of the strands in the C-grid is 2 mm and the spacing of the strands is 41 mm in the longitudinal direction and 46 mm in the transverse direction (C50 –46 x 41).

Finite Element Analysis

Introduction and Validation

Several nonlinear finite element analyses were performed to investigate the behavior of the proposed deck panels from the onset of loading to failure. The commercially available finite element analysis software Abaqus was used in all numerical simulations. The finite element models were validated based on laboratory tests performed in Florida for the deck system developed by Mirmiran et al. (2009). The results from the finite elements models were compared with Florida's test results in terms of load displacement curves, peak loads, and crack patterns at failure. Four different simulations were performed: 1) a typical T-section in a single span condition (1T1S), 2) a typical T-section in a two-span continuous condition (1T2S), 3) a simply supported panel that featured four spaces between the ribs (4T1S), and 4) a two span continuous panel that featured three spaces between the ribs (3T2S). Single symmetry and double symmetry were utilized as much as possible during the numerical simulations to reduce analysis time. Fig. 5 shows the finite element mesh, boundary conditions and the double symmetry used during the simulation of the 1T1S specimen.

3D continuum elements were used in all simulations. The size of the mesh was selected such that each element side did not exceed 13 mm in length and was determined based on results from convergence studies to provide a balance between accuracy and computational expense. The nonlinear behavior of concrete was simulated using the concrete damage plasticity approach available in Abaqus developed by Lubliner et al. (1988) and Lee and Fenves (1998). The uniaxial behavior of concrete in compression and tension as well as that for the $MMFX_2$ bars was based on the data reported by Mirmiran et al. (2009) and is provided in Fig. 6. The uniaxial tensile stress of concrete past tensile strains of 0.01 was maintained at 1 MPa to avoid convergence issues. Table 2 provides the parameters used in the concrete damage plasticity model. These parameters were based on calibration as well as on recommendations from Abaqus documentation (2016) and Malm et al. (2006). Dilation angle represents concrete's internal friction angle. Malm et al. (2006)

showed that low values of dilation angle correspond to brittle behavior, while higher values correspond to ductile behavior. The value of dilation angle used in this study is 45^{o}.

The value of eccentricity is related to the ratio between the tensile strength and compressive strength of concrete and typically is taken equal to 0.1. Therefore an eccentricity value of 0.1 was adopted in this study. σ_{b0} / σ_{c0} is the ratio of initial equibiaxial compressive yield stress to the initial uniaxial compressive yield stress. This value was assumed to be 1.77 based on the work performed by Sercombe et al. (1998). K is the ratio of the second stress invariant on the tensile meridian to that on the compressive meridian at initial yield for any given value of the pressure invariant such that the maximum principal stress is negative (Abaqus 2016). This ratio varies from 0.5 to 1.0 and a typical assumed value in the concrete damaged plasticity approach is 0.67. Therefore K was taken equal to 0.67. The viscosity parameter was assumed to be zero in this study.

Fig. 7 compares the experimental and numerical load versus mid-span displacement curves for all four specimens. The numerically obtained load versus mid-span displacement curves for specimens 1T1S, 4T1S, and 3T2S compare rather well with the experimentally obtained curves, featuring only minor differences during the entire loading. The experimental and numerical curves for 1T1S and 4T1S are almost identical. For the 1T2S specimen the curves are different up until a displacement of 13 mm. After that the curves become very similar. It should be noted that both numerical and experimental models showed an increase in stiffness for the two-span continuous configurations compared to the single span configurations with the exception of tested specimen 1T2S, which did not show this expected trend. Considering the test setup, one possible explanation for the differences between experimental and numerical load displacement curves for specimen 1T2S could be a delayed proper sitting of either the loading plate on the specimen or the specimen on the supports.

Table 3 shows a comparison of peak loads obtained analytically and experimentally. The average of the ratios between the numerically obtained peak load and that obtained experimentally is 1.00 and the coefficient of variation is 6%. In all four cases the ratios vary from 0.92 to 1.05, which indicates that the numerical models predict fairly well the capacity of the panels. Such small differences in terms of peak loads suggest that the numerical model can estimate the capacity of the precast panels with good accuracy. Additionally, a comparison between the numerically obtained principal plastic tensile strains (PE) and crack patterns observed experimentally at failure was performed for all four considered specimens. In this study the principal plastic strain contours are used to qualitatively illustrate the induced damage due to crack formation and propagation rather than provide an accurate depiction of crack patterns such as crack width, length, spacing, etc. Such an endeavor was outside the scope of this paper. The results are shown in Fig. 8. The plastic principal tensile strain contours suggest that the general location of the diagonal tension crack (shear crack) in the web of the 1T1S specimen was simulated fairly well in the numerical model. Additionally, two of the flexural cracks below the longitudinal rib marked in black in the tested specimen match those illustrated by the principal plastic strain contours at the same location in the numerical model. A diagonal shear crack was also observed during the testing of specimen 1T2S, and this was replicated in the numerical model near the intermediate support. In both specimens 1T1S and 1T2S the failure mode was one-way shear, whereas specimens 4T1S and 3T2S exhibited a combination of punching shear and yield line failure. Fig. 8 shows how the outline of the major crack on the top of the precast panels 4T1S and 3T2S was captured in the numerical simulations.

The similarity in terms of load displacement curves, peak loads, and crack patterns at failure suggests that the numerical models can simulate fairly well the behavior of the precast deck panel under monotonic loads. This modeling protocol was used in the development of the movable bridge deck panels for the state of Louisiana. The next section provides a comparison between the two proposed deck configurations in terms of load versus mid-span displacements.

Comparison of deck configurations 1 and 2

The two proposed deck configurations were loaded to failure and their performance was compared in terms of the applied load versus mid-span displacement. The investigations featured a single span deck panel simply supported at the steel stringers (Fig. 9). The edges of the panels were assumed to be free. This approach was taken to examine the relative performance of the two deck configurations under service level and ultimate level loads in a simple setup before studying the benefits of continuity and redundancy.

Ductal was used as the concrete material in both deck configurations. The uniaxial behavior of *Ductal* in compression was characterized by testing in compression cylinders of 51 mm diameter and 102 mm height, and by obtaining the full stress-strain relationship. All specimens were moist cured until the day they were tested. Fig. 10 illustrates the uniaxial stress-strain curve used in the nonlinear finite element simulations. The stress-strain curve in compression covers the range from the onset of loading to the peak load. The descending branch in compression was conservatively ignored. The measured modulus of elasticity at 28 days (E_c = 56,312 MPa), peak compressive stress (f_{cm} = 145 MPa), and the corresponding strain (ε_{cu} = 0.0026) are provided in Fig. 10. The measured compressive strength for *Ductal* at 28 days did not quite meet ACI's definition for UHPC (145 MPa versus 150 MPa) but it was only 5 MPa short of doing so.

The uniaxial behavior of *Ductal* in tension was characterized by performing splitting tensile strength tests using the approach recommended by Graybeal (2006), who concluded that an adaptation of ASTM C 496 splitting tensile test showed to provide a practical means for determining the tensile cracking strength of UHPC. The splitting tensile strength tests were conducted on cylinders of 102 mm diameter and 203 mm depth by recording the load that caused the first crack and the peak load. The peak load was always higher than the load that caused the first crack. *Ductal* was assumed to exhibit an isotropic behavior up to the formation of the first crack. The measured cracking stress (f_{tm} = 11.2 MPa) and peak stress (f_{tu} =18 MPa) at 28 days are provided in Fig. 10 and are similar to the values reported by Graybeal (2006) for untreated specimens at 28 days. The material tested by Graybeal was also the commercial product marketed by Lafarge. The strain corresponding with the peak stress (ε_{tu} = 0.0065) as well as the softening modulus (E_s = 500 MPa) were based on data from direct tensile tests performed by Park et al. (2012), who recorded both load and displacement to obtain the stress-strain relationship in tension for ultra-high performance hybrid fiber reinforced concrete. The stress-strain curve reported by Park et al. (2012) that most closely matched the first cracking and peak strength measured during this study was used to correlate the peak strength to the corresponding strain. This was done due to the fact that only loads were obtained during the splitting tensile test method. A tensile stress of 1 MPa was assumed for tensile strains exceeding 0.01 to avoid convergence issues.

The modulus of elasticity for the C-grid was assumed to be 234,430 MPa and was based on literature provided by the manufacturer. The stress-strain relationship for the C-grid was assumed to be linear, and the ultimate strain (ε_{fu}) was taken equal to 0.0099.

The bond between reinforcement bars and concrete was assumed to be perfect. To validate this assumption the computed maximum stress on the rebars computed from finite element analysis was compared with the developable stress calculated using the guidelines provided in ACI 440.1 (2006). The developable stress was calculated using Equation (1).

$$f_{fe} = \frac{0.083\sqrt{f_c'}}{\alpha}\left(13.6\frac{l_e}{d_b} + \frac{C}{d_b}\frac{l_e}{d_b} + 340\right) \leq f_{fu} \quad (1)$$

where

f'_c = design concrete compressive strength (145 MPa)

α = bar location factor (taken equal to 1.0)

l_e = embedment length of reinforcement bar, (635 mm for No. 13, No. 16, No. 19, and No. 22, 330 mm for No. 10).

d_b = diameter of reinforcement bar (10 mm for No.10, 13 mm for No.13, and 16 mm for No.16).

C = cover to the center of the bar (19 mm for No. 16, 17 mm for No.13, 11 mm for No.10).

f_{fu} =design tensile strength of FRP, considering reductions for service environment (1372 MPa for No.10, 1312 MPa for No.13, 1184 MPa for No.16).

Embedment length was calculated as the distance from the point of maximum stress in the reinforcement to the end of the reinforcement. Table 4 provides a summary of the maximum computed stress, developable stress and the ratio between the developable stress and maximum computed stress for flexural reinforcement in the longitudinal and transverse directions of the bridge. The ratio between the developable stress and maximum computed stress in the GFRP bars is higher than 1.0 for both transverse and longitudinal bars. These results validate the assumption of a perfect bond between the reinforcement bars and concrete.

Both deck configurations were loaded to failure using three different positions for the truck wheel loads namely a_1, a_2, and a_3 (Fig. 2). Position a_1 was used to maximize positive bending by locating the center of the tire print at mid-span. Position a_2 was used to maximize one-way shear effects by locating the edge of the tire print at a distance *d* (113 mm) from the internal face of stringer support. Position a_3 was intended to maximize punching shear effects, by locating the tire print in deck configuration 1 in such a way that the top flange of the deck was the only component providing resistance. In deck configuration 2 the components providing resistance are the top flange and the longitudinal ribs.

Fig. 11 shows that the performance of deck configuration 2 under the various load positions is better than that of deck configuration 1. In all cases the peak load obtained for deck configuration 2 is higher than both the service level and ultimate level loads. All numerical simulations that do not exhibit a descending branch ended at the last converged load step. Service level load (95 kN) was calculated as the load corresponding to one wheel for an HL-93 truck (71 kN) times the dynamic load allowance (1.33). The ultimate level load (166 kN) was calculated as the service level load times the live load factor of 1.75. The difference between the peak loads obtained for deck configuration 1 and 2 for tire positions a_1 and a_2 varied from 53 kN to 85 kN. For tire position a_3 the difference between the peak loads was 75 kN. Deck configuration 2 exhibited larger deflection capacity compared to deck configuration 1. Such deflection capacity is essential when the deck is subject to ultimate level loads because it provides an opportunity for the adjacent ribs or deck panels to share the load once cracking, yielding or softening takes place at the most critical location. In general, deck configuration 2 was stronger and more ductile but it also softened at lower loads. For example for load position a_1 the stiffness of the deck configuration 2 is noticeably lower than the stiffness of deck configuration 1 even for loads lower than the service level load. Because deck configuration 2 performed much better than deck configuration 1, this configuration was selected for all subsequent analyses.

The influence of tire position on the capacity of the deck panel was further examined by investigating three additional loading positions namely b_1, b_2, and b_3 on deck configuration 2 (Fig.

2). These additional tire positions match with tire positions a_1, a_2, and a_3 with respect to their locations from the stringer supports, however the wheel loads in these cases are centered over the ribs rather than in between them. Fig. 12 suggests that the peak loads for load positions *a* and *b* were generally similar. The differences in peak loads varied from 13 kN to 22 kN.

Fig. 13 illustrates the principal plastic tensile strains at failure for all load positions described so far. The black color represents principal plastic tensile strains that are equal to or greater than 0.0065, which is the strain that corresponds with the peak tensile strength measured during the material characterization study. Load position a_1 featured mid-span loading with the load placed between the transverse ribs. As a result, there is significant cracking in the flange and in the longitudinal ribs immediately underneath the load. Once the load is transferred to the transverse ribs the majority of the cracks take place in the webs of the transverse ribs due to their reduced thickness. Additionally, there are some flexural cracks in the bottom of the transverse ribs at mid-span. The overall behavior of the deck panel for this load position can be characterized as follows: flexural cracking will initiate at the bottom of longitudinal ribs followed by flexural cracking at the bottom of top flange and bottom of stem; formation of shear cracks in the stem will ensue; the ultimate condition is expected to be a shear failure of the stem.

For load position a_2 the principal plastic tensile strain contours in the flange are similar to those observed for load position a_1. However, as expected, the plastic strain contour in the webs of the transverse ribs is more pronounced in the more heavily loaded side of the span. In addition to the shear cracks in the web of the transverse ribs, there are also shear-flexural cracks at the bottom of the transverse ribs, flexural cracks near mid-span, as well as some cracking at the bottom of the transverse ribs near the support. The overall behavior of the deck panel for this load position in terms of the sequence of cracking and the ultimate condition is similar to that described for load position a_1.

For load position a_3 the cracking is concentrated in the top flange as well as in the webs of the transverse ribs. Cracking in the transverse ribs is dominated by shear cracking in the web. The failure mode for this load position is expected to be dominated by shear in the stem with the deck panel exhibiting significant flexural cracking at the bottom of the top flange.

The principal plastic tensile strain contours for load position b_1 differ from those for load position a_1 because the majority of the cracks take place in the web of the loaded transverse rib as well as in the bottom of the stem as opposed to the top flange. This is due to the fact that the load is centered over the ribs. As stated earlier, cracking in the webs of the transverse ribs is dominated by shear cracks and takes place due the reduced thickness of the web, while cracking in the bottom of the stem features flexure-shear and flexure cracks. The overall behavior of the deck panel for this load position can be characterized as follows: flexural cracking will initiate at the bottom of stem, followed by the formation of shear cracks in the stem; the ultimate condition is expected to be a shear failure of the stem.

The principal plastic tensile strain contours for load position b_2 are characterized mainly by shear cracks in the webs of the most heavily loaded transverse ribs, as well as some flexure-shear cracks and flexure cracks at the bottom of the stem. The cracking in the top flange is not as severe as it is for load position a_2 because the load is applied directly over the transverse ribs. The overall behavior of the deck panel for this load position in terms of the sequence of cracking and the ultimate condition is similar to that described for load position b_1.

Finally, the principal plastic tensile strain contours for load position b_3 suggest shear cracking in the webs of the transverse ribs near the support. The overall behavior of the deck panel for this load position is characterized by the formation of shear cracks in the stem, followed by flexural cracking at the bottom of the stem; the ultimate condition is expected to be a shear failure of the stem. The next section describes the details of a parametric study that was undertaken for deck configuration 2 to investigate the influence of a variety of parameters on the performance of the deck panel.

Parametric study

Given that deck configuration 2 showed promise in providing an alternative solution for Louisiana's movable bridge decks, the influence of a variety of parameters on the performance of the deck panel was investigated. These parameters were: 1) the addition of CFRP stirrups in the webs of the transverse ribs, 2) the influence of more than one layer of C-grid in the top flange, and 3) the influence of the uniaxial behavior of *Ductal* in tension on the behavior of the deck panel in terms of strength and stiffness. The single span deck panel simply supported at stringer locations illustrated in Fig. 9 was used for the parametric study to reduce analysis time.

Fig. 14 shows the investigated layout of CFRP shear reinforcement in the transverse ribs. The CFRP shear reinforcement consists of the C-grid used as top flange reinforcement. Loading position b_1 was used to investigate the influence of CFRP shear reinforcement on the behavior of the deck panel. Fig. 15a shows that the influence of CFRP stirrups on the performance of the deck panel is negligible. This suggests that the contribution of the CFRP shear reinforcement to the strength of the deck panel compared to the contribution of concrete is much smaller. *Ductal*'s contribution to the shear strength of the panel is provided in terms of compression struts and tension ties. The area of CFRP shear reinforcement is not large enough to make a marked difference. Accordingly, given the small thickness of the web and the fact that the placement of such shear reinforcement will require additional labor and quality control the addition of this type of shear reinforcement is not recommended.

Although all the deck panels investigated so far featured single panels simply supported at the stringer locations, the influence of the C-grid on helping the top flange distribute loads between the transverse ribs was investigated by varying the presence and amount of carbon fiber reinforcement. Three cases were analyzed: 1) no C-grid, 2) one-layer of C-grid, and 3) two layers of C-grid. Tire position a_1 was considered in all cases because it featured a load position between the transverse ribs. Fig. 15b suggests that the C-grid increases slightly the capacity of the deck panel. The difference in peak loads is 6 kips for cases that featured no grid and one layer of grid, and 3 kips for cases that featured one layer of grid and two layers of grid. Additionally, the C-grid serves as negative moment reinforcement in regions of negative moment and also helps in controlling crack widths. It is therefore recommended to include at least one layer of the C-grid as reinforcement in the top flange.

Finally, the influence of the uniaxial behavior of *Ductal* in tension on the performance of the deck panel was investigated by examining three different uniaxial tensile behaviors. One of the advantages of UHPC is that it can provide considerable resistance in tension compared to normal strength concrete. However, the behavior of UHPC in tension varies widely and depends on fiber orientation as well as the test method used to characterize this behavior. Fig. 16a illustrates the three uniaxial stress-strain relationships in tension considered for this study. The first is the tensile behavior of *Ductal* used in the study performed by Mirmiran et al. (2009), which is characterized by linear elastic behavior up until the first crack and a slight softening behavior after the first crack. The second is similar to the first except that the cracking stress is higher. The softening modulus for both of these cases was assumed to be 35 MPa and the maximum tensile strain was limited to

0.01. The cracking stress for the second tensile behavior was based on the measured value during the splitting tensile tests performed for this study. The third behavior is characterized by linear elastic behavior up until the first crack, a hardening branch between the cracking stress and the peak stress, and a softening branch past the peak tensile strength. As stated earlier the softening modulus for third case was 500 MPa and was based on data collected by Park et al. (2012). The maximum tensile strain for the third case was also limited to 0.01. For tensile strains greater than 0.01 a tensile stress of 1 MPa was assumed to avoid convergence issues.

Fig. 16b suggests that the uniaxial tensile behavior of *Ductal* affects the overall behavior of the deck panel under the applied load. The higher the cracking stress the higher the capacity of the deck panel. Additionally, the hardening behavior after the first crack leads to a higher capacity for the deck panel. While the difference in peak loads is not significant an improved uniaxial behavior in tension leads to a stiffer and slightly stronger response of the deck panel.

Effect of Continuity

All the numerical simulations performed so far were done on single span deck panels simply supported at the stringer supports. In reality the deck for the movable bridges will consist of several precast deck panels in both the longitudinal and transverse directions of the bridge. To investigate the influence of continuity on the load capacity of the deck panel a two span continuous single deck panel configuration was investigated (Fig. 17a). Various load positions were investigated with the purpose of selecting the one that leads to the lowest peak load for the two-span continuous configuration. These load positions are illustrated in Fig. 17a and feature two HL-93 truck wheel loads spaced 1.83 m apart. Each load position features wheel loads centered over the transverse ribs. This orientation of wheel loads was previously determined to result in the lowest peak load for the single span precast panels. The first two selected load positions were c_1

and c_3. Load position c_1 was expected to maximize shear stresses at the exterior left support. Load position c_3 was expected to maximize flexural positive stresses and deflections in the left span. Load position c_2 was added to capture a loading case between load position c_1 and c_3. Load position c_4 was expected to maximize shear stresses at the interior support. Load position c_5 represents a case in which half of the wheel load is supported by one panel and the other half by the adjacent panel. Fig. 17b suggests that load positions c_1, c_4, and c_5 do not control, and that the most critical cases are load positions c_2 and c_3 (i.e. when one of the wheel loads is placed near mid-span). Load position c_5 did not control because the transverse joint features two exterior reinforced ribs side by side. The differences in load displacement curves between load position c_2 and c_3 are small enough to suggest that additional load cases that feature tire positions between c_2 and c_3 are not warranted. For each load position a nonlinear finite element analysis was performed to obtain the full load versus mid-span displacement curve. These curves are illustrated in Fig. 17b. The vertical axis represents the ratio between the load applied to the deck panels and the ultimate level load for each case. In some cases only a portion of the two wheel loads could be applied to the two span continuous configuration because the spacing of the wheel loads specified in AASHTO is 1.83 m and the span length for the deck panels is 1.27 m. The load position that led to the lowest peak load was load position c_3. This load position was used to investigate the efficiency of the C-grid as negative moment reinforcement.

The influence of the C-grid as negative moment reinforcement was investigated by varying the presence and amount of the carbon fiber reinforcement in the deck panel for load position c_3 (Fig. 18a). The service level load was calculated by multiplying the portion of the wheel loads that fell on the two span continuous configuration by the dynamic load allowance (1.33). The ultimate level load was calculated by multiplying the service level load by 1.75. Fig. 18b illustrates the relationship between the total load versus the displacement at the center of the load in the left span. When no layer of C-grid is provided, the peak load (270 kN) is slightly smaller than the ultimate level load (273 kN). When one layer of C-grid is provided, the peak load is increased to 301 kN, and when two layers are provided the peak load is 319 kN. Fig. 18b suggests that there needs to be at least one layer of C-grid in the top flange to meet the ultimate load demand.

The ratio between the peak load (301 kN) obtained for load position c_3 in the two span continuous configuration and the ultimate level load (273 kN) is 1.10. This is similar and actually lower than the ratio between the peak load (187 kN) for load position b_1 in the single deck singly supported configuration and the corresponding ultimate level load (166 kN), which is 1.13. This suggests that the ultimate condition is dominated by shear failure and that continuity in the transverse direction does not help in increasing the load capacity of the deck panels. The inclusion of adjacent panels in the direction of traffic may or may not increase the load capacity of the deck system. This was not evaluated because it was outside the scope of work and because the service level and ultimate level loads were surpassed in all investigated cases. The fact that the mode of failure is primarily a shear failure is illustrated in Fig. 19a, which provides an isometric view of the two span continuous configuration from the bottom and depicts the principal plastic tensile strain contours. Regions in black represent areas in which the principal tensile plastic strain is equal to or greater than 0.0065 and are located primarily in the webs of the transverse ribs.

Finally, all load displacement curves shown so far demonstrate that the proposed deck panel configuration possesses significant deflection capacity in the nonlinear range regardless of the load position and continuity. In all investigated cases the maximum recorded deflection was at least 20 mm. The softening of the load displacement curve typically occurred at a mid-span deflection of approximately 1 mm. As a result, the proposed deck configuration offers a deflection capacity that is at least 20 times the computed elastic displacement.

Fig. 19b illustrates the principal plastic tensile strain contours at failure for the two span continuous configuration for two cases. The first case features no C-grid reinforcement in the top flange (left), and the second features one layer of C-grid in the top flange. Only the strain contours for the left span in Fig. 18a are shown. The black color represents those regions in which the plastic strain is higher than or equal to 0.0065, which is the strain that corresponds with the peak tensile strength recorded during the material characterization study. The principal tensile plastic strain contours corroborate the conclusion drawn earlier that there should be at least one layer of C-grid in the top flange. The extent of damage in terms of crack formation is more pronounced in the case that features no layers of C-grid in the top flange. As a result, the presence of the C-grid in the top flange helps control the extent of cracking in addition to increasing the load capacity of the deck panel.

Deflections

Fig. 20 shows the load versus mid-span displacement for the single span simply supported condition and load position b_1 as well as for the two span continuous configuration and load position c_3 up to and beyond service level loads. Load positions b_1 and c_3 led to maximum deflections at service for the single span and two span continuous configurations, respectively. The dashed vertical line represents the maximum allowable deflection for steel grid decks specified in Article 9.5.2 of AASHTO LFRD Specifications (2014), which was calculated as L/800. For the simply supported condition the deflection at service is 5.5 mm, which is greater than the allowable limit (1.6 mm). However, when continuity is introduced the deflection at service becomes 2.2 mm, which is 38% larger than the allowable limit. This suggests that while the introduction of continuity did not result in an increase in terms of load capacity for the panel, it resulted in an increase in stiffness. The No.16 bars in the interior transverse ribs were replaced with No.19 and No.22 bars to study their influence on the stiffness of the deck panels. Additionally, the bars in the exterior transverse ribs were changed to No. 16 for both cases. When a No.19 bar is used, the maximum deflection in the two span continuous configuration is 1.7 mm as opposed to the 1.6 mm allowable. When a No.22 bar is used the maximum deflection is 1.5 mm, which is smaller than the allowable limit. The perfect bond assumption was validated for both new bar sizes and the results are shown in Table 4. These results suggest that simply increasing the size of the bottom bars helps satisfy AASHTO's requirement for deflection. Also, it is expected that the introduction of additional panels, both, in the transverse and longitudinal directions should result in deflections that are even lower than the allowable limit.

In the light of this discussion it is recommended that the deck panels be fabricated in at least a two span continuous configuration to increase the stiffness of the system by taking advantage of the inherent continuity in such a configuration. Additionally, it is recommended that No. 22 bars be used to meet AASHTO's deflection limit. Even in cases for which AASHTO's deflection limit may not be critical to the performance of the deck system it is recommended that the deck panels be fabricated in at least a two span continuous configuration to reduce the number of joints exposed to traffic.

Conclusions and Recommendations

The development of a high performance concrete deck for movable bridges in the state of Louisiana was presented. The study was analytical in nature and consisted of several validated nonlinear finite element analyses. The primary challenge in developing this deck system was the limitation on the overall weight of the deck panel.

Two deck configurations were investigated. The first deck configuration failed to meet ultimate load demands for those load positions that maximized the effects of one-way shear and punching shear. The second deck configuration performed satisfactorily under all load positions by providing load capacities that surpassed service level and ultimate level loads. This deck configuration was used in all subsequent analyses.

Ductal produced by Lafarge North America was used as the concrete material. An improved uniaxial behavior of *Ductal* in tension appears to improve the overall behavior of the deck panel under load. GFRP bars are recommended as reinforcement for the bottom of the stem because they are light, corrosion resistant, can be fully developed in the available space, and are able to help develop the computed deck panel capacities. One layer of C-grid is recommended to be used as top flange reinforcement to provide negative moment resistance, control cracking, and distribute loads in the longitudinal direction.

The presence of the C-grid as shear reinforcement had a negligible effect on the capacity of the deck panel. Accordingly, while the proposed deck configuration satisfies AASHTO's ultimate load demand without any shear reinforcement, other potential shear reinforcement options will be considered during future research provided that shear was critical for the UHPC/HPC waffle slabs.

Continuity in the transverse direction did not result in an increase in deck panel capacity compared to the corresponding ultimate load, but it increased the stiffness of the deck system. This increase in stiffness resulted in lower deflections at service. It is recommended that the deck panels be fabricated in at least a two span continuous configuration to increase the stiffness of the system by taking advantage of the inherent continuity is such a configuration. Additionally, it is recommended that No. 22 bars be used for the interior transverse ribs to meet AASHTO's deflection limit (Article 9.5.2). Even in cases for which AASHTO's deflection limit may not be critical to the performance of the deck system it is recommended that the deck panels be fabricated in at least a two span continuous configuration to reduce the number of joints exposed to traffic.

The ultimate condition determined based on the principal plastic tensile strain contours at peak loads was dominated by shear failure in the webs of the transverse ribs, with the deck panel exhibiting flexural cracking at the bottom of the stem and bottom of the top flange. Flexural cracking in the top flange was more pronounced for those load positions which featured wheel loading between the transverse ribs.

The analytical investigations presented in this paper were based on several assumptions. Physical testing of single span and multiple span deck panels is scheduled in the near future to validate some of the assumptions made during this analytical study. Additionally, in all cases the loading was monotonic. Physical testing of the deck panels under cyclic loading will be conducted to investigate the effects of fatigue on the performance of the deck panels. Also, additional concrete mixes will be investigated and alternative deck panel configurations will be developed with the purpose of arriving at an option that provides the best balance between performance and economy.

Acknowledgments

This study was sponsored by the Louisiana Transportation Research Center (LTRC). The authors would like to thank the project review committee for their comments and their thorough review of the work performed to date. The authors would also like to thank Lafarge North America for donating *Ductal* to conduct the material characterization study. The opinions expressed herein are those of the authors and do not necessarily reflect the views of the sponsor.

References

Aaleti, S., Petersen, B., Sritharan, S. (2013). *Design Guide for Precast UHPC Waffle Deck*

Panel System, Including Connections (No. FHWA-HIF-13-032), US Department of Transportation, Federal Highway Administration, Washington D.C.

Aaleti, S., Sritharan, S., Bierwagen, D., Wipf, T., (2011). “Structural behavior of waffle bridge deck panels and connections of precast Ultra-High-Performance Concrete: Experimental Evaluation”, Transportation Research Record, *Journal of the Transportation Research Board*, (2251), pp.82-92.

AASHTO (American Association of State Highway and Transportation Officials). (2014). *AASHTO LRFD Bridge Design Specifications* 6th Edition. Washington, DC.

Abaqus [Computer Software]. Dassault Systèmes Americas Corp., Waltham, MA.

Abaqus. (2016). *User's Manual Version 6.14-2*. Dassault Systemes Simulia Corp.

ACI (American Concrete Institute). (2015). “Ultra-High Performance Concrete”, *ACI 239-15*, Farmington Hills, MI.

ACI (American Concrete Institute). (2006). “Guide for the Design and Construction of Structural Concrete Reinforced with FRP Bars”, *ACI 440.1R-06*, Farmington Hills, MI.

ACI (American Concrete Institute). (2013). “ACI Concrete Terminology”, *ACI CT-13*, Farmington Hills, MI.

ASTM (American Society of Testing Materials). (2010). “Standard test method for splitting tensile strength of cylindrical concrete specimens”, *ASTM C496*, West Conshohocken, PA. C496

Chomarat North America, Anderson, SC. [http://www.chomarat.com/en/category/ produits/ produits-produits/c-grid/?from=technologie], (Accessed March 2016).

Gase, P.M. (2008). ”Prefabricated Steel Grid Bridge Decks”, [https://www.dot.state.oh.us/ engineering/OTEC/2008%20Presentations/55C.pdf] (Accessed March 2016)

Graybeal, B.A. (2006). “Practical Means for Determination of the Tensile Behavior of Ultra-High

Performance Concrete”, *Journal of ASTM International*, Vol. 3, No. 8.

Lee, J., Fenves, G. L. (1998). “Plastic-Damage Model for Cyclic Loading of Concrete Structures”, *Journal of Engineering Mechanics*, 124 (8), 892–900.

Lubliner, J., Oliver, J., Oller, S., Oñate, E. (1989). “A Plastic-Damage Model for Concrete,” *International Journal of Solids and Structures*, 25 (3), 229–326.

Malm, R., James, G., Sundquist, H. (2006). “Monitoring and evaluation of shear crack initiation and propagation in webs of concrete box-girder section”, *International Conference on Bridge Engineering Challenges in the 21st Century*, Hong Kong.

Menkulasi, F., Parker, J., Montes, C., Baghi, H., Sandrock, J.P., Gomez, S. (2016). “Development of a Sustainable UHPC Deck for Movable Bridges”, *1st International Interactive Symposium on Ultra-High Performance Concrete*, Des Moines, IA, July 18-20, DOI: 10.21838/uhpc.2016.84.

Mirmiran, A., Ghasemi, S. (2016). “Lightweight Solid Decks for Movable Bridges – Phase II”, Final Report, Florida Department of Transportation Research Center, FDOT Contract No. BDV29-977-11, January, Tallahassee, FL.

Mirmiran, A., Saleem, M., A., Mackie, K., Xia, J. (2009). “Alternatives to steel grid decks” Draft Final Report, Florida Department of Transportation Research Center, FDOT Contract No. BD015RPWO#22, Tallahassee, FL.

Mirmiran, A., Saleem, M., A., Mackie, K., Xia, J. (2012). “Alternatives to steel grid decks – Phase II”, Final Report, Florida Department of Transportation Research Center, FDOT Contract No. BDK80 977-06, Tallahassee, FL.

Park, S. H., Kim, D. J., Ryu, G. S., Koh, K. T. (2012). “Tensile behavior of ultra-high performance hybrid fiber reinforced concrete", *Cement and Concrete Composites*, 34(2), 172-184.

Phillips, J. (2014). "Bascule Bridge Lightweight Solid Deck Retrofit Research Project", Florida Department of Transportation, Project Status Report, Tallahassee, FL.

Sercombe, J., Toutlemonde, F., J.ULM, F. (1998). "From material behavioral to structural design for concrete in high rate dynamics", *Computational Modelling of Concrete Structures*, Balkema, Rotterdam, ISBN 90 5410 9467.

Table 1 Recommendations for UHPC deck panel

Recommendations		Reason/Comment
Description	Value	
Panel Thickness (mm)	132	To be consistent with predominant existing grid deck thicknesses
Max. Panel weight (kN/m^2)	0.96	Calculated based on stringer reactions
Max. Span length (m)	1.27	It covers the majority of existing steel grid deck spans
Continuity	3+	Min. of three spans or simple span made continuous
Stringer	W410×54	Most common stringer

Table 2 Parameters for concrete damage plasticity model

Parameter	Value
Dilation angle (degrees)	45
Eccentricity	0.10
$\frac{\sigma_{bo}}{\sigma_{co}}$	1.77
K	0.67
Viscosity parameter	0

Table 3 Comparison of peak loads obtained numerically and experimentally

Specimen Description	Peak Loads (kN)		Ratio = P_{Num}/P_{Exp}
	Numerical	Experimental	
1T1S	168	182	0.92
1T2S	248	246	1.01
4T1S	387	377	1.03
3T2S	686	656	1.05
			Average = 1.00
			COV = 0.06

Table 4 Computed stress versus developable stress

Type	Size	Transverse			Longitudinal		
		f_{fe} (MPa)	$f_{computed}$ (MPa)	$f_{fe}/f_{computed}$	f_{fe} (MPa)	$f_{computed}$ (MPa)	$f_{fe}/f_{computed}$
GFRP	No.10				852	690	1.24
	No.13	1064	830	1.28			
	No.16	926	758	1.22			
	No.19	822	634	1.30			
	No. 22	750	482	1.55			

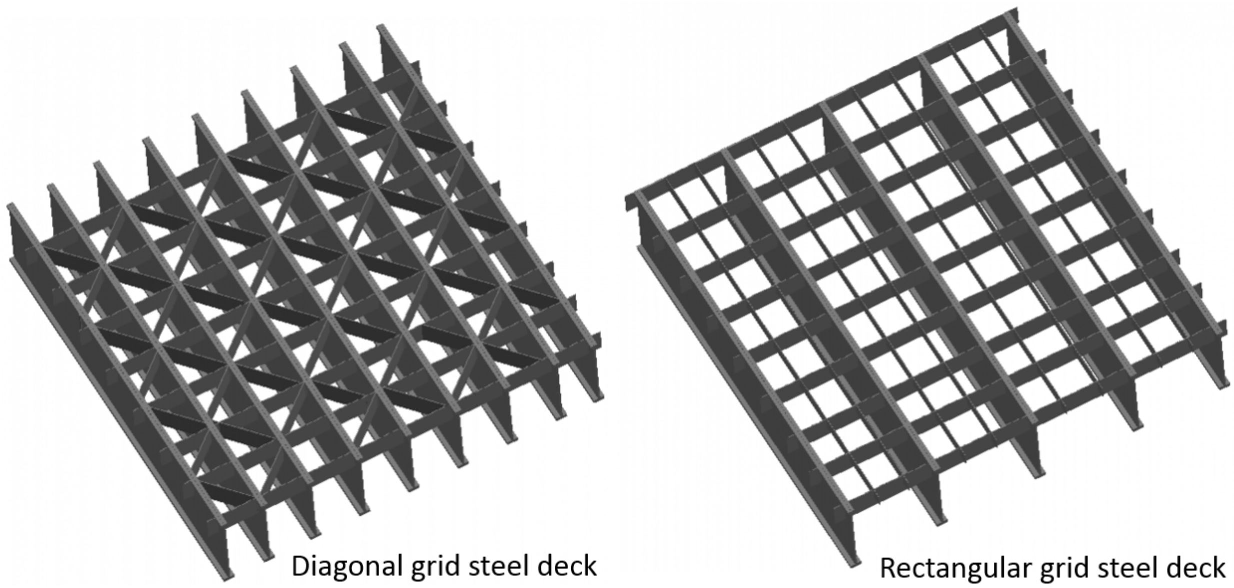
Diagonal grid steel deck
Rectangular grid steel deck

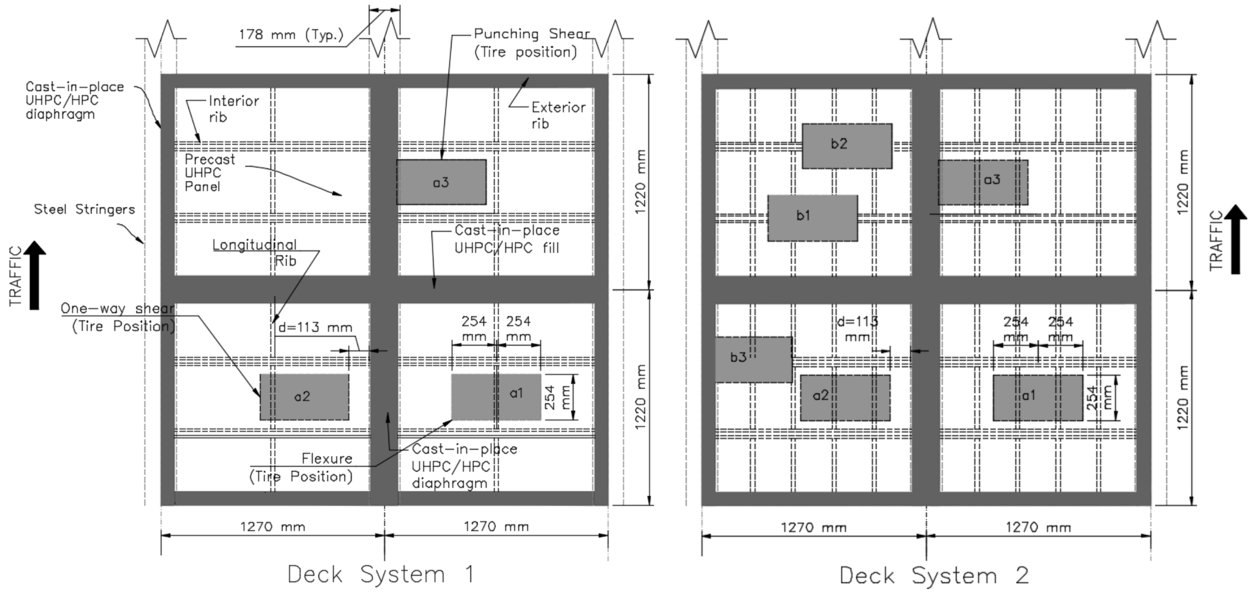

a) Single span precast deck panels

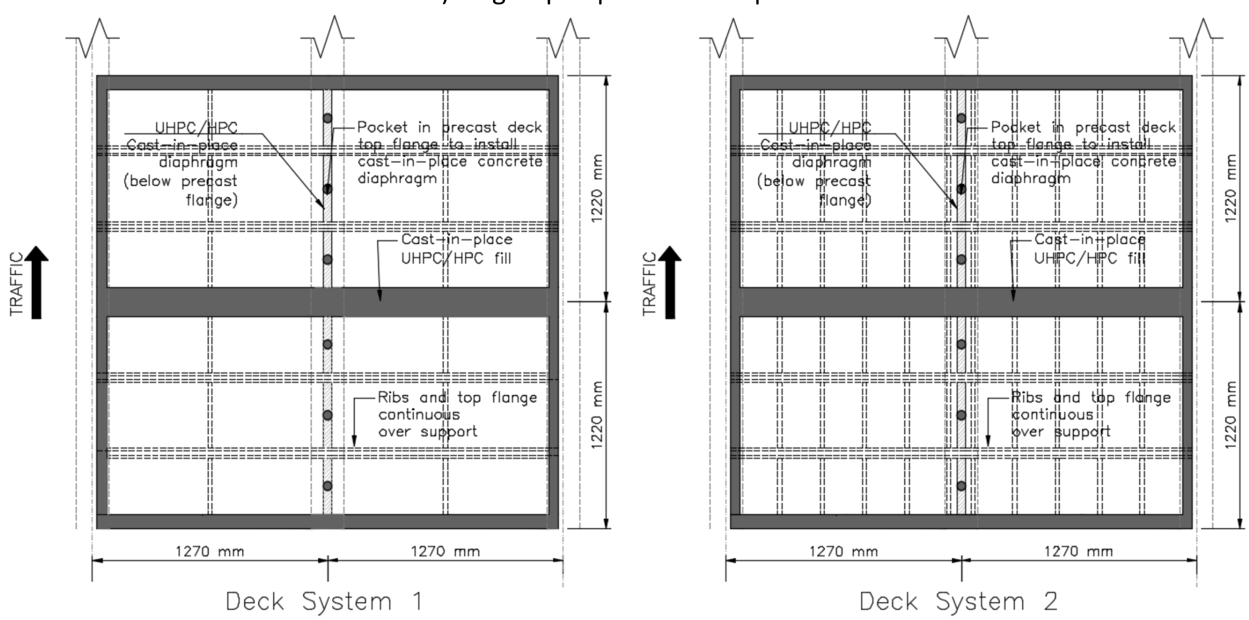

b) Two-span continuous precast deck panels

Figure

Click here to download Figure Fig. 3.pdf

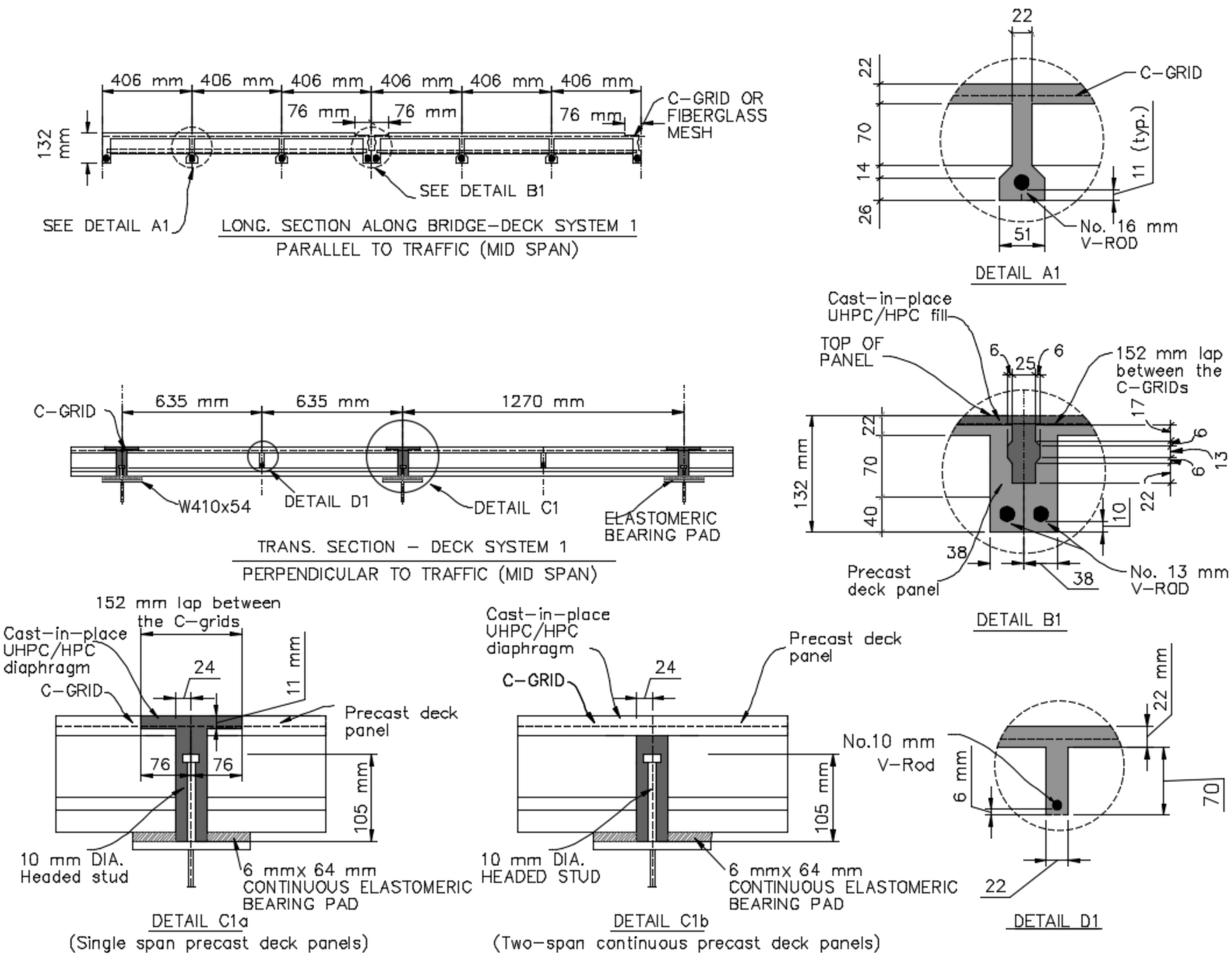

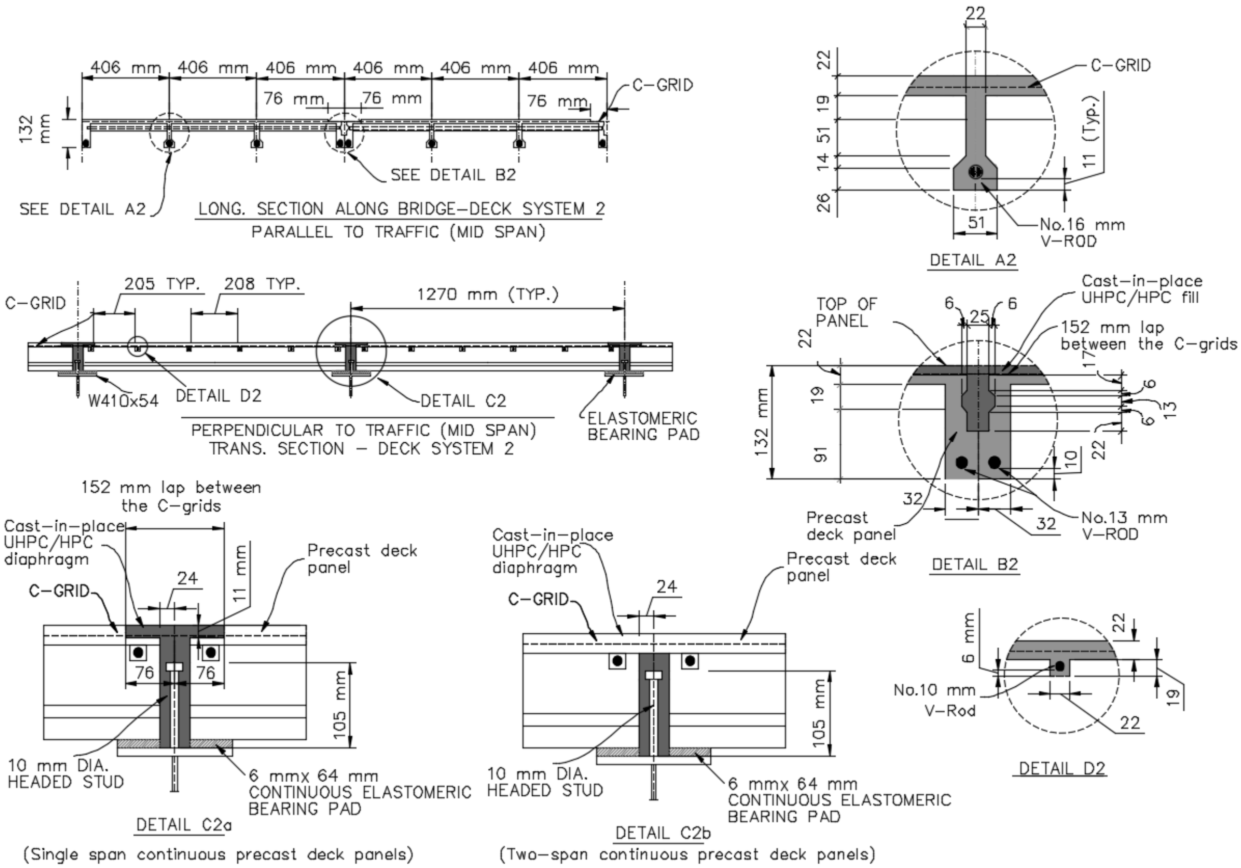
406 mm 406 mm 406 mm 406 mm 406 mm 406 mm
76 mm 76 mm 76 mm
C-GRID
132 mm
SEE DETAIL B2
SEE DETAIL A2
LONG. SECTION ALONG BRIDGE-DECK SYSTEM 2
PARALLEL TO TRAFFIC (MID SPAN)
C-GRID
205 TYP. 208 TYP.
1270 mm (TYP.)
W410x54
DETAIL D2
DETAIL C2
ELASTOMERIC BEARING PAD
PERPENDICULAR TO TRAFFIC (MID SPAN)
TRANS. SECTION – DECK SYSTEM 2
C-GRID
11 (Typ.)
No.16 mm V-ROD
DETAIL A2
TOP OF PANEL
Cast-in-place UHPC/HPC fill
152 mm lap between the C-grids
Precast deck panel
No.13 mm V-ROD
DETAIL B2
152 mm lap between the C-grids
Cast-in-place UHPC/HPC diaphragm
C-GRID
Precast deck panel
105 mm
10 mm DIA. HEADED STUD
6 mmx 64 mm CONTINUOUS ELASTOMERIC BEARING PAD
DETAIL C2a
(Single span continuous precast deck panels)
Cast-in-place UHPC/HPC diaphragm
C-GRID
Precast deck panel
10 mm DIA. HEADED STUD
6 mmx 64 mm CONTINUOUS ELASTOMERIC BEARING PAD
DETAIL C2b
(Two-span continuous precast deck panels)
No.10 mm V-Rod
DETAIL D2

Figure

Click here to download Figure Fig. 5.pdf

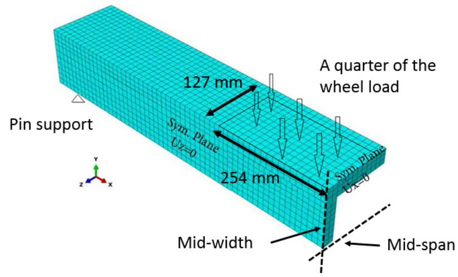

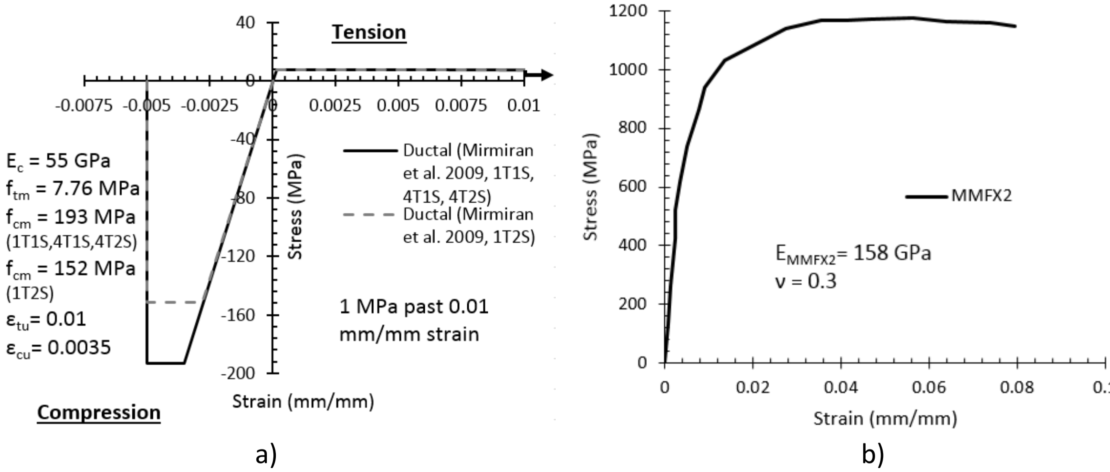
Tension
Compression
Stress (MPa)
Strain (mm/mm)
Ductal (Mirmiran et al. 2009, 1T1S, 4T1S, 4T2S)
Ductal (Mirmiran et al. 2009, 1T2S)
E_c = 55 GPa
f_tm = 7.76 MPa
f_cm = 193 MPa (1T1S,4T1S,4T2S)
f_cm = 152 MPa (1T2S)
ε_tu= 0.01
ε_cu= 0.0035
1 MPa past 0.01 mm/mm strain
a)
MMFX2
E_MMFX2= 158 GPa
ν = 0.3
Stress (MPa)
Strain (mm/mm)
b)

Figure

Click here to download Figure Fig. 7.pdf

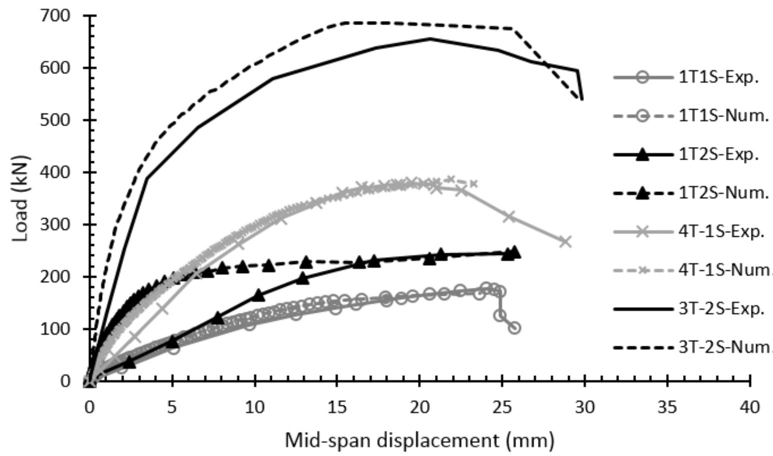

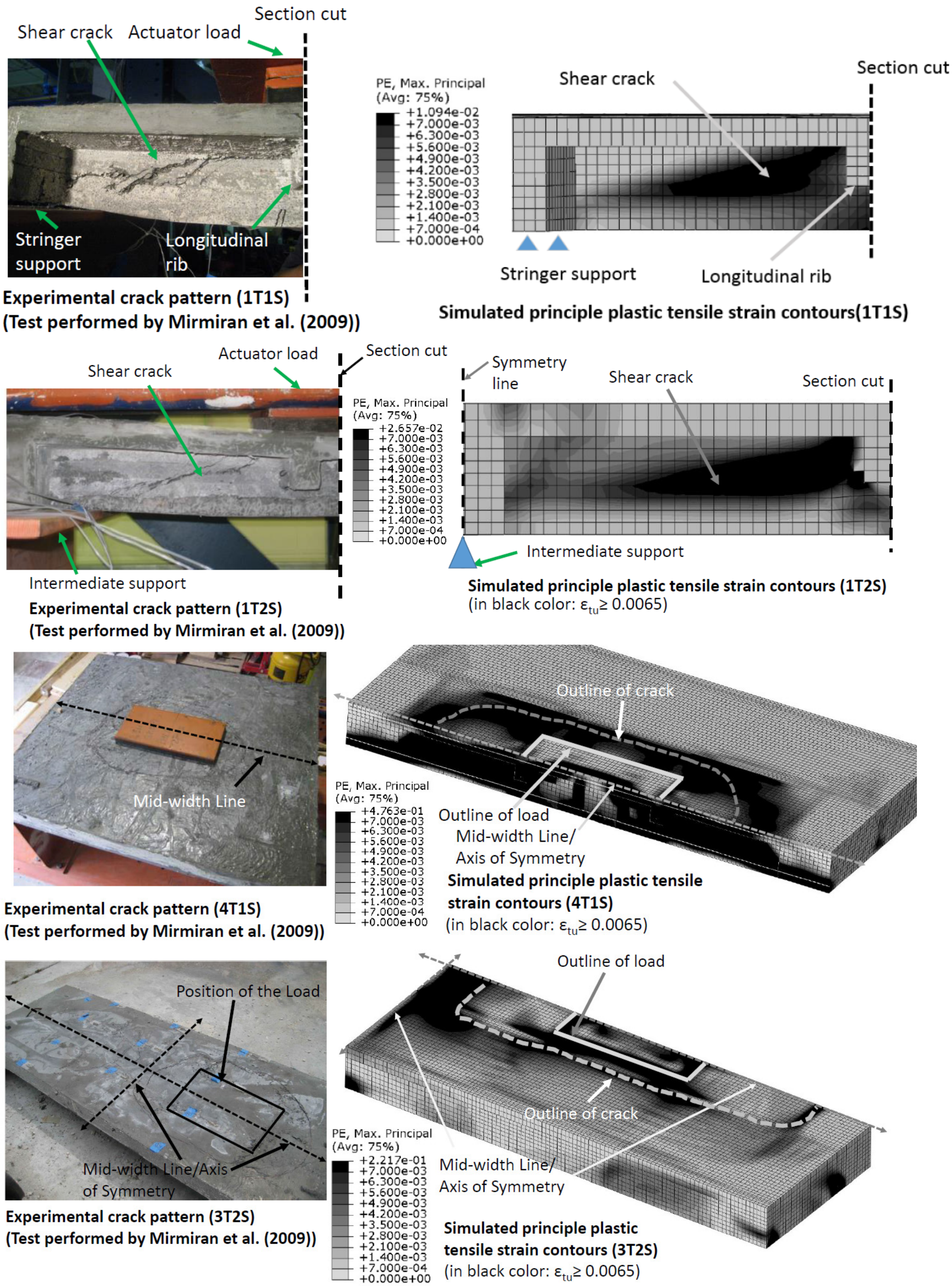
Section cut
Shear crack
Actuator load
Stringer support
Longitudinal rib
Experimental crack pattern (1T1S)
(Test performed by Mirmiran et al. (2009))
PE, Max. Principal
(Avg: 75%)
+1.094e-02
+7.000e-03
+6.300e-03
+5.600e-03
+4.900e-03
+4.200e-03
+3.500e-03
+2.800e-03
+2.100e-03
+1.400e-03
+7.000e-04
+0.000e+00
Shear crack
Section cut
Stringer support
Longitudinal rib
Simulated principle plastic tensile strain contours(1T1S)
Actuator load
Section cut
Shear crack
Intermediate support
Experimental crack pattern (1T2S)
(Test performed by Mirmiran et al. (2009))
PE, Max. Principal
(Avg: 75%)
+2.657e-02
+7.000e-03
+6.300e-03
+5.600e-03
+4.900e-03
+4.200e-03
+3.500e-03
+2.800e-03
+2.100e-03
+1.400e-03
+7.000e-04
+0.000e+00
Symmetry line
Shear crack
Section cut
Intermediate support
Simulated principle plastic tensile strain contours (1T2S)
(in black color: $\varepsilon_{tu} \geq 0.0065$)
Mid-width Line
Experimental crack pattern (4T1S)
(Test performed by Mirmiran et al. (2009))
Outline of crack
PE, Max. Principal
(Avg: 75%)
+4.763e-01
+7.000e-03
+6.300e-03
+5.600e-03
+4.900e-03
+4.200e-03
+3.500e-03
+2.800e-03
+2.100e-03
+1.400e-03
+7.000e-04
+0.000e+00
Outline of load
Mid-width Line/
Axis of Symmetry
Simulated principle plastic tensile strain contours (4T1S)
(in black color: $\varepsilon_{tu} \geq 0.0065$)
Position of the Load
Mid-width Line/Axis of Symmetry
Experimental crack pattern (3T2S)
(Test performed by Mirmiran et al. (2009))
Outline of load
Outline of crack
PE, Max. Principal
(Avg: 75%)
+2.217e-01
+7.000e-03
+6.300e-03
+5.600e-03
+4.900e-03
+4.200e-03
+3.500e-03
+2.800e-03
+2.100e-03
+1.400e-03
+7.000e-04
+0.000e+00
Mid-width Line/
Axis of Symmetry
Simulated principle plastic tensile strain contours (3T2S)
(in black color: $\varepsilon_{tu} \geq 0.0065$)

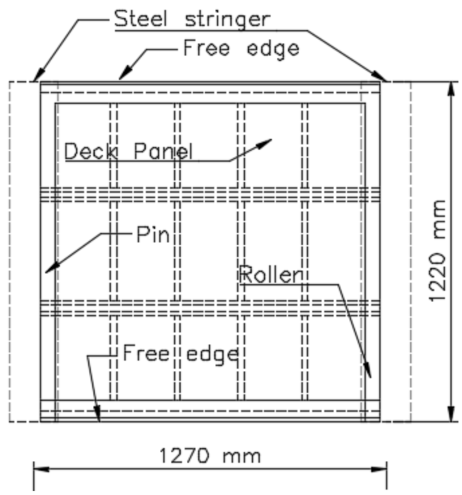
Steel stringer
Free edge
Deck Panel
Pin
Roller
Free edge
1220 mm
1270 mm

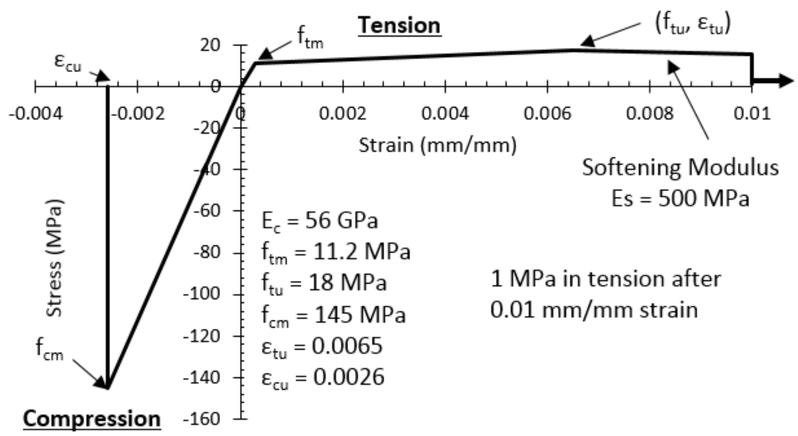
Tension
f_{tm}
$(f_{tu}, \varepsilon_{tu})$
ε_{cu}
20
0
-20
-40
-60
-80
-100
-120
-140
-160
-0.004
-0.002
0
0.002
0.004
0.006
0.008
0.01
Strain (mm/mm)
Stress (MPa)
Softening Modulus
Es = 500 MPa
E_c = 56 GPa
f_{tm} = 11.2 MPa
f_{tu} = 18 MPa
f_{cm} = 145 MPa
ε_{tu} = 0.0065
ε_{cu} = 0.0026
1 MPa in tension after
0.01 mm/mm strain
f_{cm}
Compression

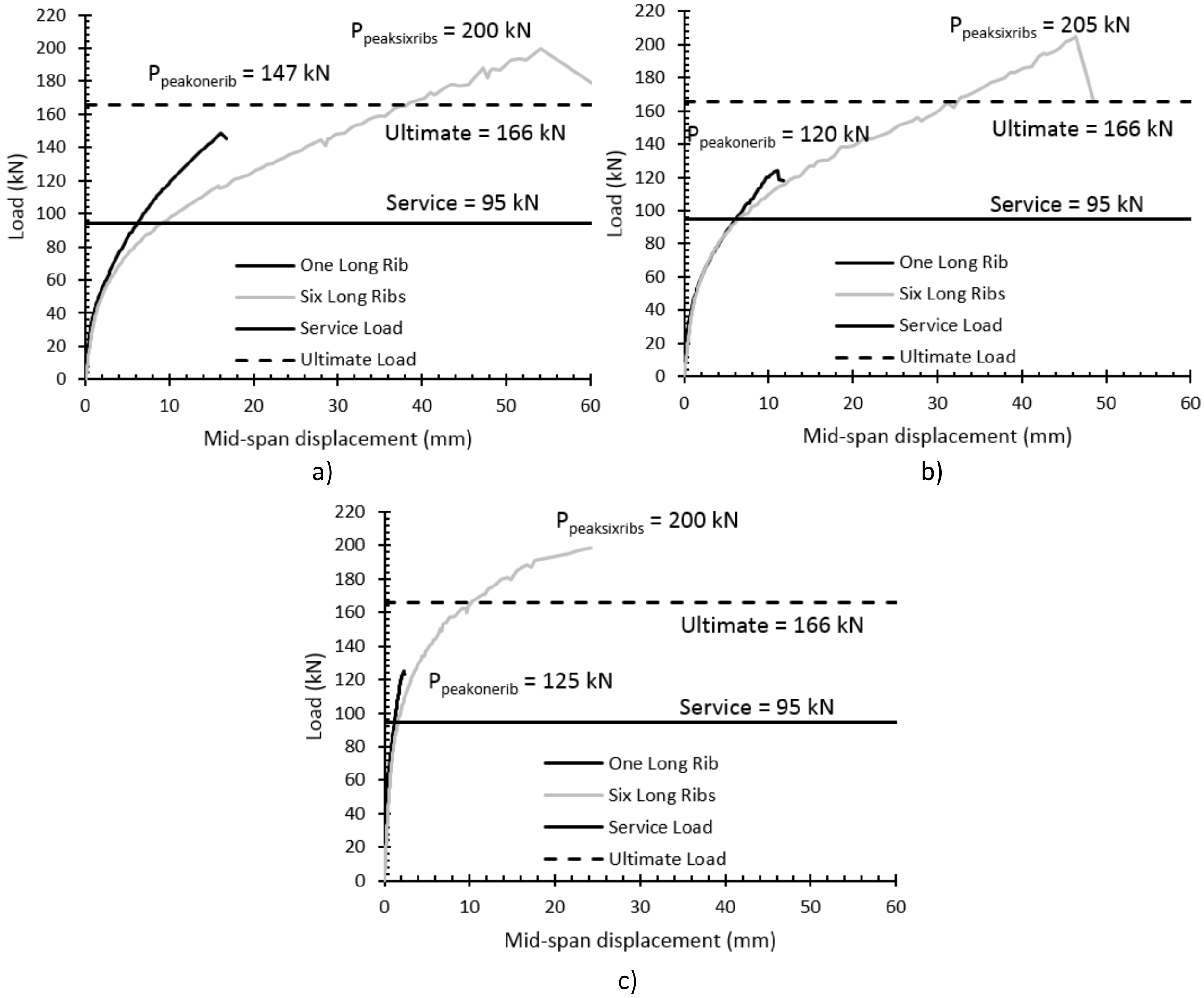
P peaksixribs = 200 kN
P peakonerib = 147 kN
Ultimate = 166 kN
Service = 95 kN
One Long Rib
Six Long Ribs
Service Load
Ultimate Load
Load (kN)
Mid-span displacement (mm)
a)
P peaksixribs = 205 kN
P peakonerib = 120 kN
Ultimate = 166 kN
Service = 95 kN
One Long Rib
Six Long Ribs
Service Load
Ultimate Load
Load (kN)
Mid-span displacement (mm)
b)
P peaksixribs = 200 kN
Ultimate = 166 kN
P peakonerib = 125 kN
Service = 95 kN
One Long Rib
Six Long Ribs
Service Load
Ultimate Load
Load (kN)
Mid-span displacement (mm)
c)

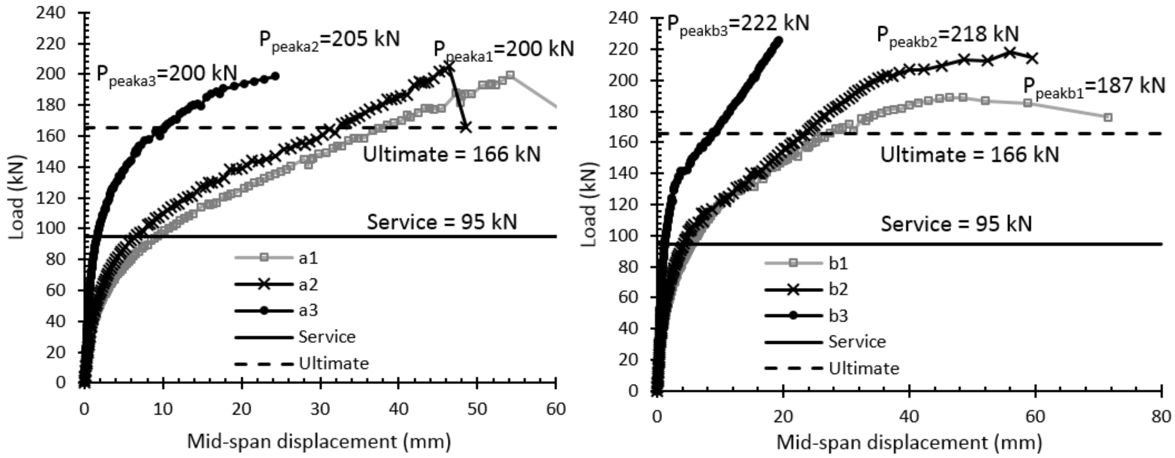
240
220
200
180
160
140
120
100
80
60
40
20
0
Load (kN)
0
10
20
30
40
50
60
Mid-span displacement (mm)
P_{peaka3}=200 kN
P_{peaka2}=205 kN
P_{peaka1}=200 kN
Ultimate = 166 kN
Service = 95 kN
a1
a2
a3
Service
Ultimate
240
220
200
180
160
140
120
100
80
60
40
20
0
Load (kN)
0
20
40
60
80
Mid-span displacement (mm)
P_{peakb3}=222 kN
P_{peakb2}=218 kN
P_{peakb1}=187 kN
Ultimate = 166 kN
Service = 95 kN
b1
b2
b3
Service
Ultimate

a) b)

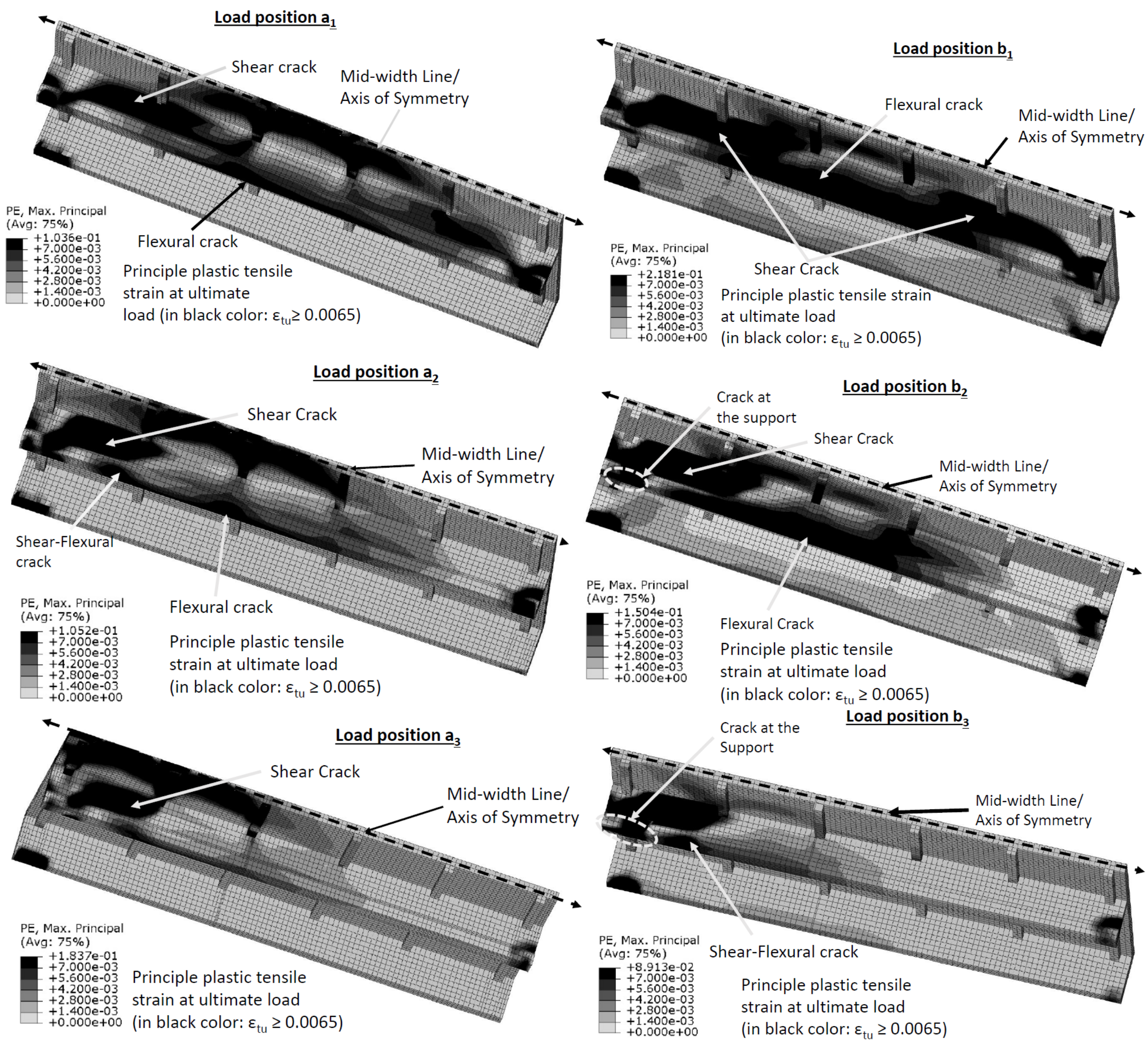

Load position a1
Shear crack
Mid-width Line/ Axis of Symmetry
Flexural crack
PE, Max. Principal (Avg: 75%)
+1.036e-01
+7.000e-03
+5.600e-03
+4.200e-03
+2.800e-03
+1.400e-03
+0.000e+00
Principle plastic tensile strain at ultimate load (in black color: εtu≥ 0.0065)
Load position b1
Flexural crack
Mid-width Line/ Axis of Symmetry
Shear Crack
PE, Max. Principal (Avg: 75%)
+2.181e-01
+7.000e-03
+5.600e-03
+4.200e-03
+2.800e-03
+1.400e-03
+0.000e+00
Principle plastic tensile strain at ultimate load (in black color: εtu ≥ 0.0065)
Load position a2
Shear Crack
Mid-width Line/ Axis of Symmetry
Shear-Flexural crack
Flexural crack
PE, Max. Principal (Avg: 75%)
+1.052e-01
+7.000e-03
+5.600e-03
+4.200e-03
+2.800e-03
+1.400e-03
+0.000e+00
Principle plastic tensile strain at ultimate load (in black color: εtu ≥ 0.0065)
Load position b2
Crack at the support
Shear Crack
Mid-width Line/ Axis of Symmetry
Flexural Crack
PE, Max. Principal (Avg: 75%)
+1.504e-01
+7.000e-03
+5.600e-03
+4.200e-03
+2.800e-03
+1.400e-03
+0.000e+00
Principle plastic tensile strain at ultimate load (in black color: εtu ≥ 0.0065)
Load position a3
Shear Crack
Mid-width Line/ Axis of Symmetry
PE, Max. Principal (Avg: 75%)
+1.837e-01
+7.000e-03
+5.600e-03
+4.200e-03
+2.800e-03
+1.400e-03
+0.000e+00
Principle plastic tensile strain at ultimate load (in black color: εtu ≥ 0.0065)
Load position b3
Crack at the Support
Mid-width Line/ Axis of Symmetry
Shear-Flexural crack
PE, Max. Principal (Avg: 75%)
+8.913e-02
+7.000e-03
+5.600e-03
+4.200e-03
+2.800e-03
+1.400e-03
+0.000e+00
Principle plastic tensile strain at ultimate load (in black color: εtu ≥ 0.0065)

Figure

Click here to download Figure Fig. 14.pdf

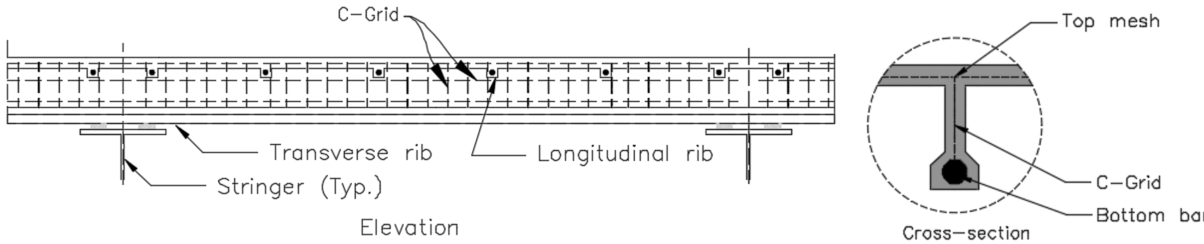

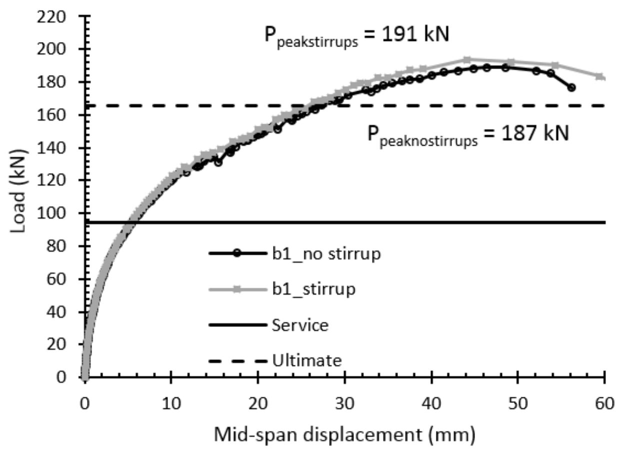
$P_{peakstirrups}$ = 191 kN
$P_{peaknostirrups}$ = 187 kN
Load (kN)
Mid-span displacement (mm)
b1_no stirrup
b1_stirrup
Service
Ultimate
0
20
40
60
80
100
120
140
160
180
200
220
0
10
20
30
40
50
60

a)

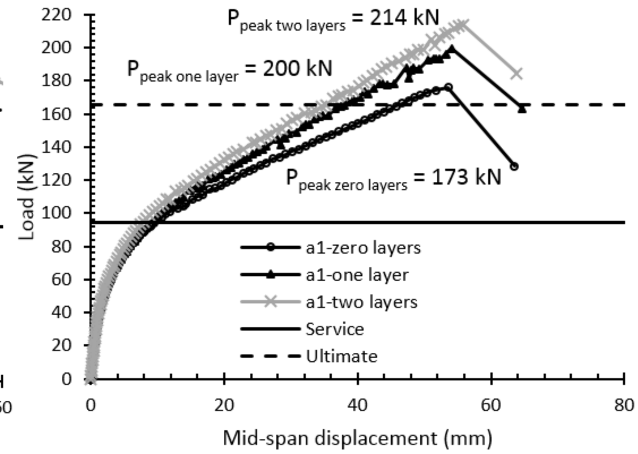
$P_{peak\ two\ layers}$ = 214 kN
$P_{peak\ one\ layer}$ = 200 kN
$P_{peak\ zero\ layers}$ = 173 kN
Load (kN)
Mid-span displacement (mm)
a1-zero layers
a1-one layer
a1-two layers
Service
Ultimate
0
20
40
60
80
100
120
140
160
180
200
220
0
20
40
60
80

b)

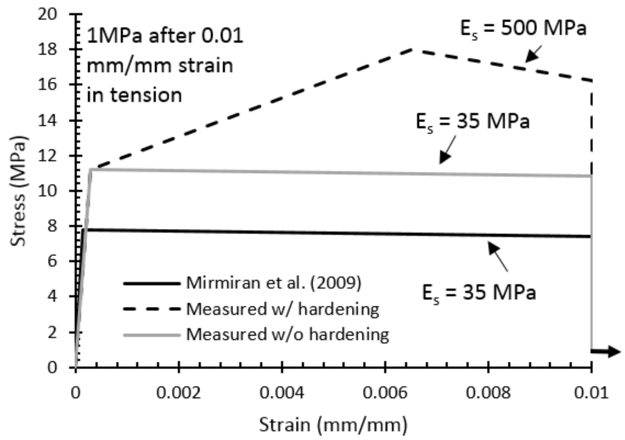
1MPa after 0.01 mm/mm strain in tension
Es = 500 MPa
Es = 35 MPa
Es = 35 MPa
Mirmiran et al. (2009)
Measured w/ hardening
Measured w/o hardening
Stress (MPa)
Strain (mm/mm)

a)

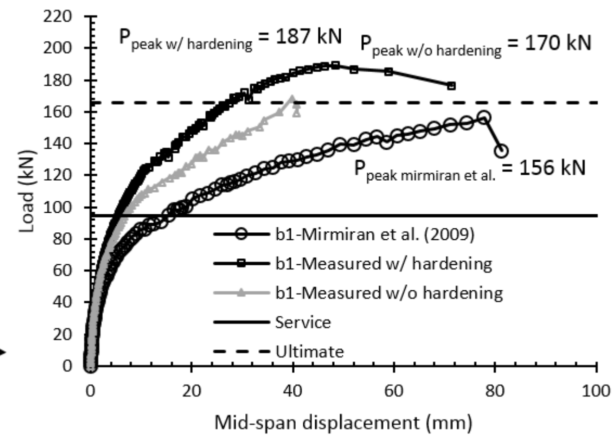
P peak w/ hardening = 187 kN
P peak w/o hardening = 170 kN
P peak mirmiran et al. = 156 kN
b1-Mirmiran et al. (2009)
b1-Measured w/ hardening
b1-Measured w/o hardening
Service
Ultimate
Load (kN)
Mid-span displacement (mm)

b)

Figure

Click here to download Figure Fig. 17.pdf

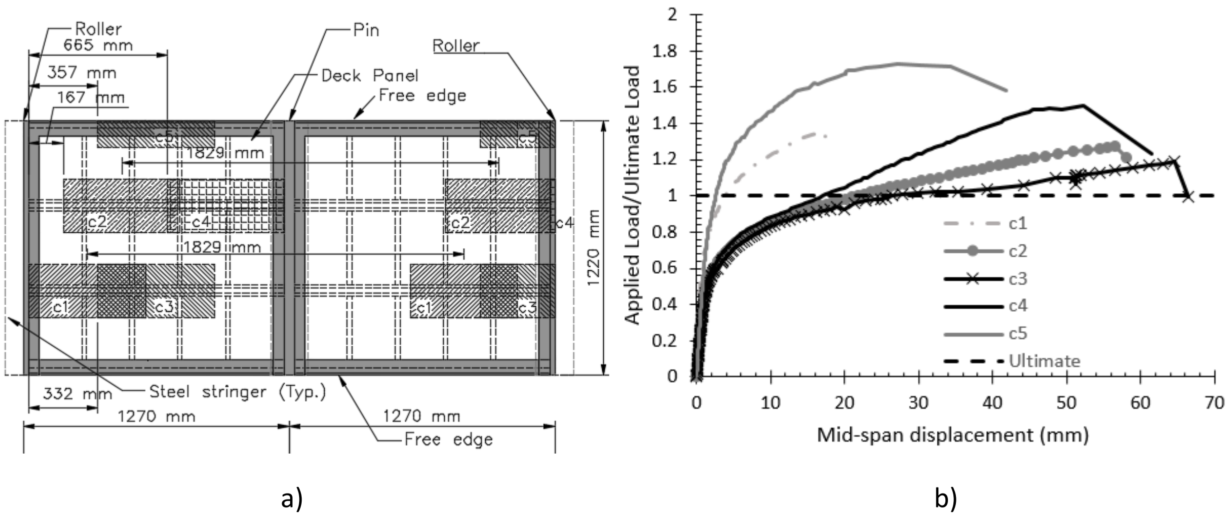

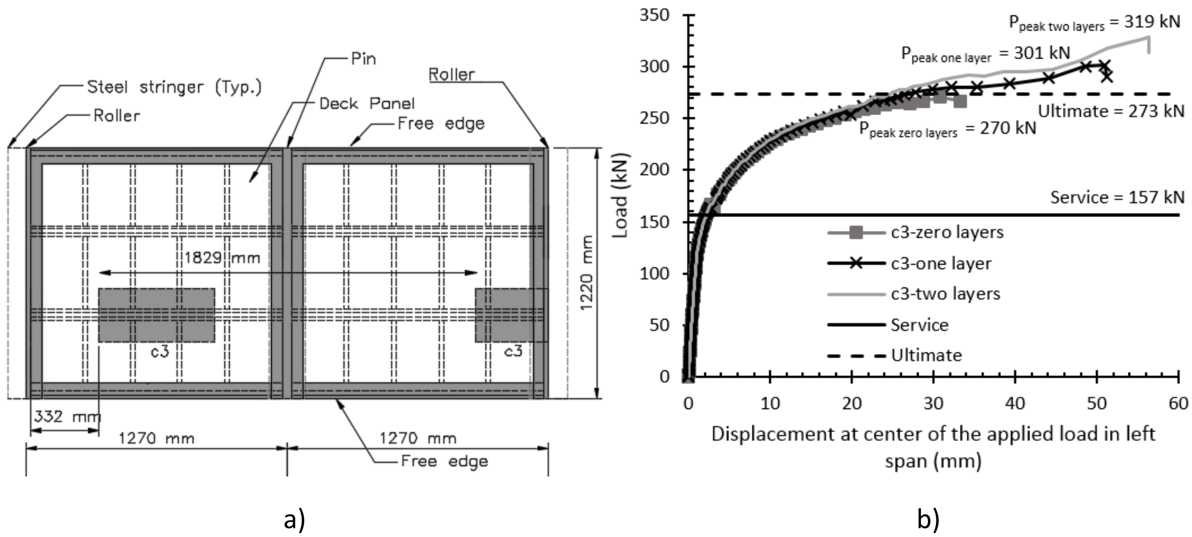
Steel stringer (Typ.)
Roller
Pin
Deck Panel
Roller
Free edge
1829 mm
c3
c3
1220 mm
332 mm
1270 mm
1270 mm
Free edge
a)
P peak two layers = 319 kN
P peak one layer = 301 kN
Ultimate = 273 kN
P peak zero layers = 270 kN
Service = 157 kN
c3-zero layers
c3-one layer
c3-two layers
Service
Ultimate
Load (kN)
Displacement at center of the applied load in left span (mm)
b)

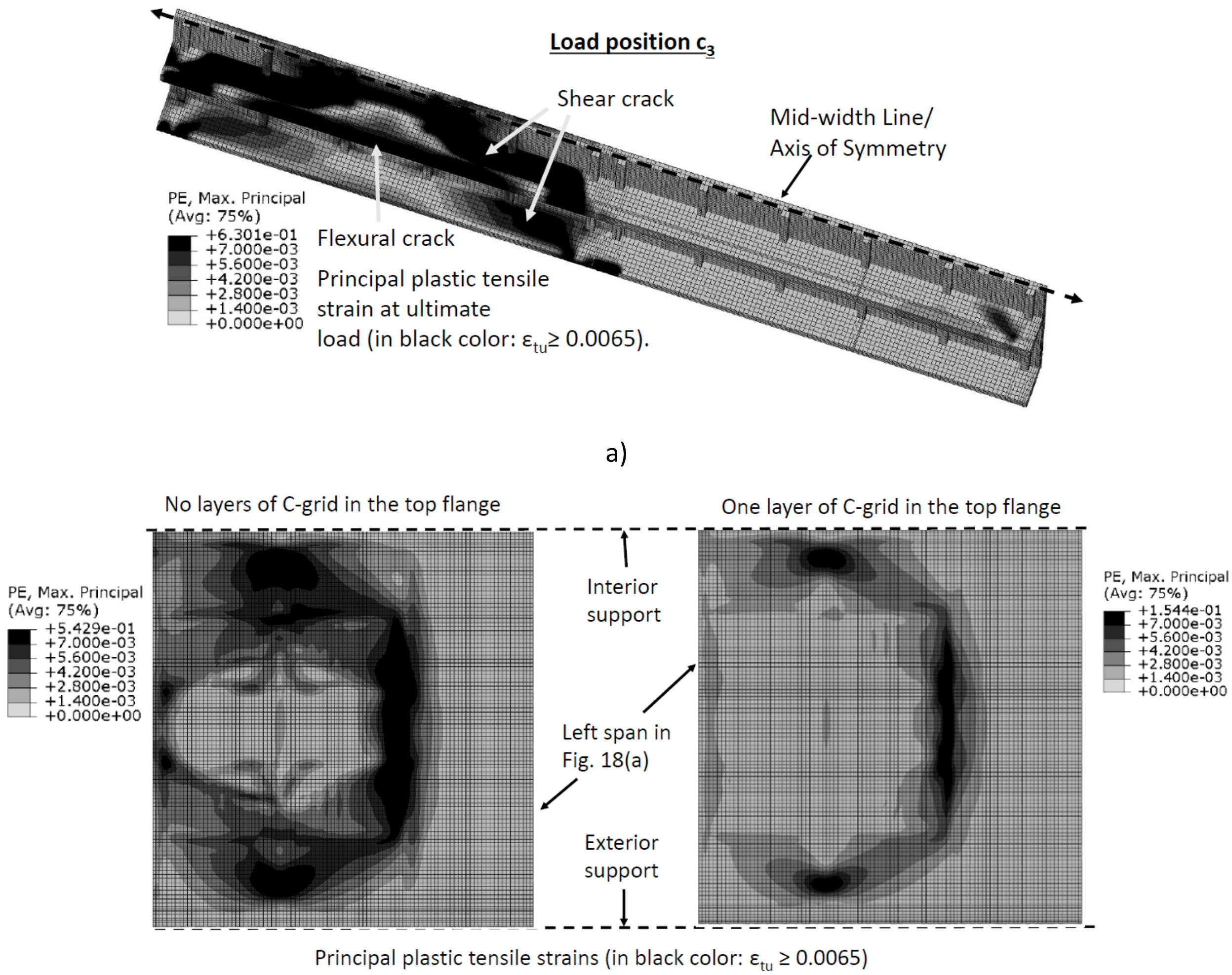
Load position c_3
Shear crack
Mid-width Line/
Axis of Symmetry
PE, Max. Principal
(Avg: 75%)
+6.301e-01
+7.000e-03
+5.600e-03
+4.200e-03
+2.800e-03
+1.400e-03
+0.000e+00
Flexural crack
Principal plastic tensile
strain at ultimate
load (in black color: $\varepsilon_{tu} \geq 0.0065$).
a)
No layers of C-grid in the top flange
One layer of C-grid in the top flange
PE, Max. Principal
(Avg: 75%)
+5.429e-01
+7.000e-03
+5.600e-03
+4.200e-03
+2.800e-03
+1.400e-03
+0.000e+00
Interior
support
Left span in
Fig. 18(a)
Exterior
support
PE, Max. Principal
(Avg: 75%)
+1.544e-01
+7.000e-03
+5.600e-03
+4.200e-03
+2.800e-03
+1.400e-03
+0.000e+00
Principal plastic tensile strains (in black color: $\varepsilon_{tu} \geq 0.0065$)

b)

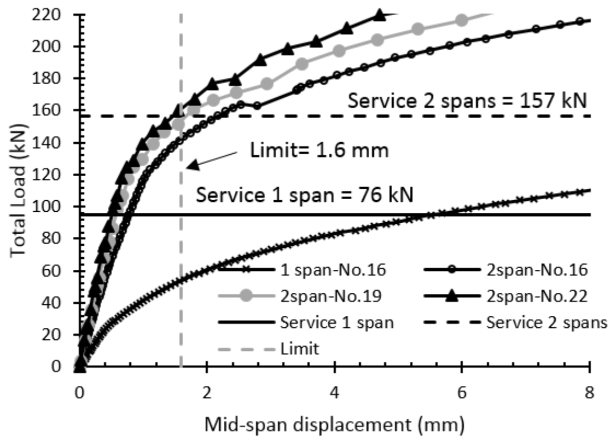

Service 2 spans = 157 kN
Limit= 1.6 mm
Service 1 span = 76 kN
Total Load (kN)
Mid-span displacement (mm)
1 span-No.16
2span-No.16
2span-No.19
2span-No.22
Service 1 span
Service 2 spans
Limit

List of Figures

Fig. 18 a) Most critical position of wheel loads for two span continuous case, b) Load versus mid-span displacement for various layers of CFRP mesh in the top flange

Fig. 19 Principal plastic tensile strains at failure for two span continuous configuration, a) isometric view, b) top view

Fig. 20 Performance at service